Project no. GOCE-CT-2003-505539

Project acronym: ENSEMBLES

Project title: ENSEMBLE-based Predictions of Climate Changes and their Impacts

Instrument: Integrated Project

Thematic Priority: Global Change and Ecosystems

Deliverable Reference Number: D2A2.3

Title:
Final report on Stream 1 and Stream 2 simulations of the 20th century

Due date of deliverable: June 2008
Actual submission date: 31 December 2009

Start date of project: 1 September 2004 Duration: 60 Months

Organisation name of lead contractor for this deliverable: Danish Meteorological Institute and University of Copenhagen (associated partner), then CNRM

Revision [draft]

Project co-funded by the European Commission within the Sixth Framework Programme (2002-2006)		
Dissemination Level		
PU	Public	X
PP	Restricted to other programme participants (including the Commission Services)	
RE	Restricted to a group specified by the consortium (including the Commission Services)	
CO	Confidential, only for members of the Consortium (including the Commission Services)	

Final report on Stream 1 and Stream 2 simulations of the 20th century

Jean-Francois Royer, David Salas and Sophie Tyteca
CNRM / Météo France, Toulouse, France

Eigil Kaas[1]*, University of Copenhagen*

Wilhem May and Shuting Yang
DMI, Copenhagen

Ulrich Cubasch, Heike Huebener and Falk Niehörster
Freie Universität, Berlin, Germany

Jean-Louis Dufresne
Lab. Météo. Dynamique (LMD/IPSL), Paris, France

Tim Johns, Jason Lowe and Peter Good
Met Office Hadley Centre, Exeter, UK

Elisa Manzini, Pier Giuseppe Fogli, Silvio Gualdi and Enrico Scoccimarro
Istituto Nazionale di Geofisica e Vulcanologia, Centro
Euro-mediterraneo per i Cambiamenti Climatici, Bologna, Italy

Erich Roechner, Monika Esch and Wolfgang Müller
Max-Planck Institut für Meteorologie, Hamburg, Germany

Helge Drange, Odd Helge Otterå
Bjerknes Centre for Climate Research, Bergen, Norway

Bjørg Rognerud, University of Oslo, Norway

Key words: ENSEMBLES EU-project, 20th Century simulations, Stream 1 and stream 2, radiative forcing, CERA data-base.

[1] Corresponding author address: Eigil Kaas, Niels Bohr Institute, Juliane Maries Vej 30, DK-2100, Copenhagen, Denmark.
E-mail: kaas@gfy.ku.dk

Stream 1 and Stream 2 simulations of the 20th century

Abstract

The present report provides a technical overview of the "Stream 1 and Stream 2" 20th century simulations in the ENSEMBLES project. The report includes the following components:

- The experimental setups.
- Description of the models that have been used.
- The forcing and driving input data used in the different simulations.
- A few key results from stream 1 and stream 2
- A brief note on how the data can be accessed.

The report complements, and partly builds upon, the ENSEMBLES deliverable D2A.0.4, which describes the Stream 2 experimental design, and the major milestone report MM2A.2 on the provision of updated climate hindcasts of the 20th century for Stream 2.

1 Introduction

Historical simulations covering the 20th century are crucial for evaluating the ability of climate models to reproduce the general observed climate evolution, optionally also including the global carbon cycle in some simulations. In order to provide this type of model validation one of the main objectives in the ENSEMBLES project has been to produce multi-model sets of climate hindcasts (Work package WP2A.2).

The model simulations have been performed in two streams. The first set of simulations (Stream 1), has been performed using the existing atmosphere-ocean-sea ice models available at the start of the project. These can be considered state-of-the-art (approximately anno 2005) benchmark multi-model simulations, which have been used for the IPCC AR4 simulations (Solomon et al, 2007).

The second set of simulations (Stream 2) has been performed using more comprehensive Earth System Models (ESMs). For this, all model versions have been improved compared to the Stream 1 simulations. The model updates and forcings relative to Stream 1 differ from model to model and cover improvements of aerosol treatment, inclusion of or the improvement of carbon cycle models, inclusion of changing ozone concentrations, and inclusion of variable land use cover. This means that a multi-model ensemble of simulations with further developed ESMs of different complexity has been performed with the atmospheric concentrations/emissions of chemical compounds and land-use changes as forcings.

In addition to the coupled climate model/ESM simulations, a set of off-line simulations have been performed with a global atmospheric chemistry transport model at University of Oslo (**UiO**), Oslo, Norway. In this way estimates of the varying ozone concentrations have been obtained.

The present report includes a brief description of the model versions used, of the Stream 1 and Stream 2 simulations, and of some results from these simulations.

The modelling centres that have contributed to the WP2A.2 simulations are:

- Met Office, Hadley Centre for Climate Prediction and Research (**METO-HC**), Exeter, UK
- Météo-France, Centre National de Recherches Meteorologiques, (**CNRM**), Toulouse, France
- Centre National de la Recherche Scientifique, Institut Pierre-Simon Laplace (**IPSL**), Paris, France
- Danish Meteorological Institute (**DMI**), Copenhagen, Denmark
- Istituto Nazionale di Geofisica e Vulcanologia (**INGV**), Centro Euro-Mediterraneo per i Cambiamenti Climatici, Bologna, Italy
- Max-Planck Institut für Meteorologie (**MPI**), Hamburg, Germany
- Freie Universität Berlin, (**FUB**), Berlin, Germany
- Nansen Environmental and Remote Sensing Center, (**NERSC**), Bergen, Norway

The acronyms marked with bold text will also be used in following to refer to model simulations although the individual model names are different.

2 Experimental setup

The design of the experiments was made in such a way as to avoid the so called “cold start” problem which may arise when the coupled models start from an initial condition in which the atmosphere and ocean are not satisfactorily balanced (Hasselmann et al 1993). The resulting drift period has to be removed from the actual climate simulations as it can interfere with the climate change one wants to simulate. In order to minimize this problem a careful methodology has been devised for the ENSEMBLES global simulations.

For each model, the 20th century simulations were initiated from a balanced condition taken from a long control integration with constant atmospheric concentrations for greenhouse gases corresponding to the estimated forcing conditions for a preindustrial state (year 1860 conditions) for which a climate equilibrium can be assumed. For Stream 1 and Stream 2 two sets of simulations have been performed by the GCM-modelling centres:

1) A historical simulation with observed anthropogenic forcings only (greenhouse gases, aerosols and ozone concentrations) over the period 1860-2000.

2) A second historical simulation similar to the previous simulation but including, in addition, the estimated natural forcings (solar and volcanic).

For Stream 2 the first set of simulations was mandatory while the second set was optional and has, therefore, not been performed for all models.

Although all simulations were initialised from an initial state supposed to be balanced for forcing conditions at 1860 some models show a significant climate drift, i.e. the control run global mean temperature is not quasi-constant. Therefore, when analysing and using the 20^{th} century simulations that are performed with such models it can be recommended to remove this drift. For a given model the drift can be derived by the continuing the control simulation into the 20^{th} century. Note that the models are different in Stream 1 and 2. Therefore any estimates of model control climate and related drifts must be evaluated individually for the two streams.

3 Climate models used

3.1 Summary presentation of the models

The coupled climate models/ESMs used for the 20th century simulations are listed in Table 1 (Stream 1) and Table 2 (Stream 2). The first column gives the name of the model, and a few fundamental characteristics of the different models are given in the other columns.

Model name	Modelling centres	Atmosphere AGCM	Atmos. Resol.	Atm. levels	Ocean OGCM	resolution.	O. levels
HadCM3 HadGEM1	METO-HC	HadAM3 HadGAM1	2.5x3.75° 1.25x1.875°	19 38	HadOM3 HadGOM1	1.25x1.25 0.33-1°	20 40
IPSL-CM4	IPSL +UCL-ASTR	LMDZ-4	2.5x3.75°	19	ORCA	0.5-2°	31
ECHAM5/MPI-OM	MPI +DMI	ECHAM5	T63	31	MPI-OM	1.5°	40
EGMAM	FUB	ECHAM4	T30	19/39	HOPE-G	0.5-2.8°	20
INGV-SX	INGV-CMCC	ECHAM4.6	T106	19	OPA8.2	0.5-2°	31
CNRM-CM3	CNRM	ARPEGE-Climat v3	T63	45	OPA8.1	0.5-2°	31
BCCR-BCM2.0	NERSC	ARPEGE-Climat v3	T63	31	MICOM 2.8 (modified)	0.5-2°	35

***Table 1**: Models used in the ENSEMBLES Stream 1 simulations*

Model	Modelling centre	Atmos. Resolution	Atmos. levels	Ocean resolution	Ocean levels
HadGEM2-AO	METO-HC	1.25x1.875°	38	0.33-1°	40
HadCM3C	METO-HC	2.50x3.75°	38	0.4-1.5°	20
IPSLCM4_v2 IPSL-LOOP	IPSL (+ UCL-ASTR)	2.50x3.75° 2.50x3.75°	19 19	0.5-2° 0.5-2°	31 31
ECHAM5-C	MPI (+ DMI)	T31	19	3°	40
EGMAM2	FUB	T30	39	T42	20
INGV-CE	INGV-CMCC	T31	19	0.5-2°	31
CNRM-CM3.3	CNRM (+DMI)	T63	31	0.5-2°	31
BCM2 BCM2-C	NERSC	T63	31	1.5°	31

***Table 2:** Models used in the ENSEMBLES Stream 2 simulations*

All the climate models have a similar structure, where an atmospheric GCM is coupled to an ocean GCM, inclusing a sea-ice model. The atmospheric GCMs can be grouped in two families according to the numerical method used in their dynamical core: the grid-point models based on finite-difference methods for the horizontal solution of the dynamical equations (HadGEM1, HadGEM2-AO, HadCM3, HadCM3C, IPSL-CM4, IPSL-LOOP), and the spectral models using a spherical harmonics representation of the horizontal fields (ECHAM5, EGMAM+, CNRM-CM3, BCM2). In the spectral models the resolution is expressed by the maximum wavenumber represented in a triangular truncation in spectral space. The truncations used here are either low resolution (T30 or T31) or medium resolution (T63, or T106). The spectral models used can be grouped in two families: those derived from different versions of the ECHAM model (ECHAM5, ECHAM5-C, EGMAM+, INVG-SX, INVG-CE), and those from the ARPEGE-Climat model (CNRM-CM3, BCM2, BCM2-C).

3.2 Detailed Model descriptions

Detailed descriptions of the models that have contributed to the ENSEMBLES Stream 1 (ES1) simulations can be found in the CMIP3 presentation on the PCMDI site (http://www-pcmdi.llnl.gov/ipcc/model_documentation/ipcc_model_documentation.php). For convenience the links to the specific models descriptions are provided in Table 3.

Model	Link to model documentation (in html format)
HadCM3 **HadGEM1**	http://www-pcmdi.llnl.gov/ipcc/model_documentation/HadCM3.htm http://www-pcmdi.llnl.gov/ipcc/model_documentation/HadGEM1.htm
IPSL-CM4	http://www-pcmdi.llnl.gov/ipcc/model_documentation/IPSL-CM4.htm
ECHAM5/MPI-OM	http://www-pcmdi.llnl.gov/ipcc/model_documentation/ECHAM5_MPI-OM.htm
ECHAM4 – HOPE-G	(not in CMIP3)
INGV-SXG	http://www-pcmdi.llnl.gov/ipcc/model_documentation/INGV-SXG.htm
CNRM-CM3	http://www-pcmdi.llnl.gov/ipcc/model_documentation/CNRM-CM3.htm
BCCR-BCM2.0	http://www-pcmdi.llnl.gov/ipcc/model_documentation/BCCR_BCM2.0.htm

Table 3*: Links to Stream 1 model documentation on the CMIP3 website at PCMDI*

The models participating in stream 2 (ES2) are generally improved or extended versions of models that contributed to CMIP3 (through improvements to core physical schemes, inclusion or improvement of aerosol, the carbon cycle and variable land vegetation cover components). In addition to the key features listed in Table 2, a more detailed presentation of the Stream 2 models is given in the following descriptions provided by the different modelling teams, focussing particularly on the differences to the respective Stream 1 versions.

METOHC: HadGEM2-AO model

The HadGEM2-AO model is based on the HadGEM1 model used in IPCC AR4, described by Johns et al. (2006), but contains several improvements and modifications as described in Collins at el. (2008). The representation of aerosols and aerosol processes is notably improved (Bellouin et al. 2007) and both secondary organic aerosol and mineral dust are now included; both the deep and shallow convection schemes are modified leading to significant improvements in diabatic heating

profiles and moist processes; boundary layer and land surface process parametrizations are refined; the ocean Laplacian viscosity function is revised, leading to lower viscosity in the tropics; the ocean background vertical diffusivity is lower in the upper 1000m leading to reduced mixing with cooler water at depth and raising SSTs; and a number of bug corrections are also included relative to HadGEM1.

METOHC: HadCM3C model

The HadCM3C model (Booth et al. 2009) is a modified configuration of the HadCM3 model (Gordon et al. 2000; Pope et al. 2000) used in IPCC AR4. Unlike HadCM3, it is flux adjusted (using an updated algorithm based on that described in Collins et al. (2008) and includes interactive terrestrial vegetation and an ocean carbon cycle. Externally imposed (anthropogenic) land use change cannot currently be included. The model differs from HadCM3LC (Cox et al. 2000) and the coupled carbon cycle climate model submitted to C4MIP (Friedlingstein et al. 2006), as it is configured to run with the standard (higher) HadCM3 resolution ocean (1.25°x1.25°) and also includes interactive atmospheric sulphur cycle chemistry and sulphate aerosol scheme with direct and indirect aerosol effects

IPSL: IPSL-CM4 model

The IPSL-CM4 model has been used in IPCC AR4 and its main components are the following: LMDZ4 atmosphere (Hourdin et al. 2006); ORCHIDEE land and vegetation (Krinner et al. 2005); OPA8.2 ocean (Madec et al. 1999); LIM sea ice (Timmermann et al. 2005); OASIS3 coupler (Valcke 2006). The version used for stream 2 contains some improvements: the horizontal resolution has been increased (Marti et al., 2009) and land use change may be externally imposed. As in Dufresne et al. (2005), sulphate aerosols concentration are externally imposed, the direct and indirect aerosols are considered. The ozone concentration is not modified and the effect of volcanoes is considered via a change of the solar constant.

IPSL: IPSL-LOOP model

IPSL-CM4-LOOP (Cadule et al. 2009) results of the coupling between the IPSL-CM4 coupled ocean-atmosphere general circulation model (Marti et al. 2009) and the two carbon cycle models: PISCES (Pelagic Interactions Scheme for Carbon and Ecosystems Studies) biogeochemical model (Aumont et al., 2003) for the ocean part and ORCHIDEE (ORganizing Carbon and Hydrology in Dynamic EcosytEms) model for the terrestrial part (Krinner et al. 2005). PISCES includes 3 nutrients, 2 phytoplanktons, 2 zooplanktons, one detritus and semi-labile dissolved organic matter. It explicitly represents the collimation of phytoplankton growth by light and three nutrients:phosphate, iron and silicate. The phytoplankton reservoir is split in two sizes fractions corresponding to nano-phytoplankton and diatoms. Two sizes of zooplankton (micro-plankton and mesozooplankton) are also explicitly considered. ORCHIDEE is a dynamic global vegetation model (DGVM) which calculates energy and hydrology budgets, carbon assimilation, allocation and decomposition and vegetation competition. ORCHIDEE distinguishes 13PFTs amongst which the natural and agricultural vegetation distributions are prescribed. In every grid point different PFTs can coexist.

MPI+DMI: ECHAM5-C model

The model used for the stream2 simulations is a low-resolution version of the Max Planck Institute for Meteorology Earth System Model (MPI-ESM), consisting of submodels for the atmosphere including the land surface, the ocean including sea ice, and the marine and terrestrial carbon cycle. In the atmosphere model (ECHAM5; Roeckner et al. 2006), vorticity, divergence, temperature, and the logarithm of surface pressure are represented by truncated series of spherical harmonics at a horizontal resolution of T31 (corresponding to a latitude-longitude grid of 3.75°). The advection of water vapor, cloud liquid water, and cloud ice are treated by a flux-form semi-Lagrangian scheme. A hybrid sigma/pressure system is used in the vertical direction (19 layers with the top model level at 10 hPa). ECHAM5 includes detailed parameterizations for shortwave and longwave radiation, stratiform clouds, cumulus convection, turbulent diffusion, land surface processes, and gravity wave drag.

The ocean model (MPI-OM; Marsland et al. 2003) uses the primitive equations for a hydrostatic Boussinesq fluid with a free surface. The vertical discretization is on 40 z-levels, and the bottom topography is resolved by means of partial grid cells. The ocean has a nominal resolution of 3° and the poles of the curvilinear grid are shifted to land areas over Greenland and Antarctica, respectively. The parameterizations of physical processes include along-isopycnal diffusion, horizontal tracer mixing by advection with unresolved eddies, vertical eddy mixing, near-surface wind stirring, convective overturning, and slope convection. Concentration and thickness of sea ice are calculated by means of a dynamic and thermodynamic sea ice model.

In the coupled atmosphere-ocean model (Jungclaus et al. 2006), the ocean passes to the atmosphere the sea surface temperature (SST), sea ice concentration, sea ice thickness, snow depth on ice, and the ocean surface velocities. Then the atmosphere runs with these boundary values for one coupling time step (one day), accumulates heat and fresh water fluxes (including river runoff and glacier calving), separately for ice-covered and open water partitions of the grid cells, and transfers this information to the ocean. Additionally, the 10m wind speed is passed to the ocean for the calculation of the turbulent wind mixing. The model does not employ flux adjustments.

The carbon cycle model coupled to the climate model comprises the ocean biogeochemistry model HAMOCC5 (Maier-Reimer et al. 2005) and the modular land surface scheme JSBACH (Raddatz et al. 2007). HAMOCC5 simulates photosynthesis and zooplankton grazing in the euphotic layer, depending on the nutrients nitrate, phosphate, silicate and iron. Furthermore, denitrification, nitrate fixation, and the formation of calcium carbonate and opaline shells are included. The export of detritus out of the euphotic zone results from the death of phyto- and zooplankton as well as fecal pellets.

JSBACH includes a photosynthesis module for C3 and C4 plants. Besides the photosynthetic pathway, 12 plant functional types (PFT) are distinguished by maximum carboxylation rate, maximum electron transport rate, specific leaf area carbon content, and phenotype. The biomass is allocated to a wood pool, a pool representing active plant tissue (leaves, fine roots etc.) and a pool representing sugar and starch buffering periods with negative net primary productivity. Soil carbon is partitioned into a pool with a short (about 1 year) and one with a long turnover time (about 100 years). It is released to the atmosphere by heterotrophic respiration, which is depending linearly on soil moisture and exponentially on soil temperature. Vegetation phenology is differentiated according to five phenotypes: evergreen, summergreen, raingreen forest or shrubland, grassland, and managed (non-forest) areas.

The geographic vegetation distribution is prescribed annually from maps indicating the fractional coverage of each PFT in a grid cell. For the historical period, the changes in natural land cover are based on the reconstruction of agricultural areas such as cropland and pasture (Pongratz et al. 2008). For the future scenarios, changes in agricultural extent according to the IMAGE scenario maps (http://www.mnp.nl/image/image_products/) are superimposed upon the present-day map. For both periods the geographic distribution of natural vegetation is altered by agricultural activity only and does not change with climate. The anthropogenic land cover change leads to a relocation of carbon between the pools, with part of the vegetation carbon directly released to the atmosphere, and part being transferred to the two soil pools. This scheme describes consistently the temporal evolution of land carbon storage for agricultural expansion as well as abandonment with subsequent regrowth of natural vegetation (Pongratz et al. 2009).

Owing to the long spinup required for the carbon cycle, the stream2 model had to be run at lower resolution in both the atmosphere (T31L19) and the ocean (3°L40) than the atmosphere-ocean model applied for the stream1 simulations (T63L31/1.5°L40).

FUB: EGMAM+ model

The experiments of the Free University of Berlin were run with the modified coupled atmosphere-ocean GCM **E**CHO-**G** with **M**iddle **A**tmosphere **M**odel (EGMAM) (Huebener et al. 2007). EGMAM is based on ECHO-G (Legutke and Voss 1999), which couples the ECHAM4 (Roeckner et al. 1996) in a horizontal resolution of T30 via OASIS with the HOPE-G (Hamburg Ocean Primitive Equation-Global Model) (Wolff et al. 1997) in a horizontal resolution of 0.5-2.8° (refinement near equator) and 20 vertical layers. It includes a dynamic-thermodynamic sea ice model and time constant flux correction for heat and freshwater exchange. With the extension to middle atmosphere up to 0.01 hpa (ca. 80 km) the model has 39 vertical layers and a gravity wave parameterisation (Manzini and McFarlane 1998). The model was used with an interactive aerosol transport scheme (Feichter et al. 1996), changing land use (crop, pasture) and a time varying 3d ozone field.

INGV: ECHAM5-OPA-C model

The INGV-CMCC Earth System Model (INGVCE) consists of an atmosphere-ocean-sea ice physical core coupled to a land-and-ocean carbon cycle model. The technical detail of the physical atmosphere ocean coupling and of the implementations of the vegetation and biogeochemistry (i.e., the carbon cycle part) models into the physical core model are described in Fogli et al. (2009). The role of the ocean carbon cycle in the regulation of anthropogenic carbon emission as simulated by the INGVCE model is discussed in Vichi et al. (2009). The ESM components are: ECHAM5 atmosphere (Roeckner et al. 2006); SILVA land and vegetation (Alessandri, 2006); OPA8.2 ocean (Madec et al. 1999); LIM sea ice (Timmermann et al., 2005), and PELAGOS biogeochemistry (Vichi et al. 2007). The software used to couple the atmosphere (including the land-vegetation model) model and the ocean (including the biogeochemistry) model is OASIS3 (Valcke 2006).

CNRM+DMI: CNRM-CM3 model

The CNRM-CM3 coupled general circulation model is the updated version of CNRM-CM2 (Royer et al. 2002). It consists of four main components: ARPEGE-Climat 3, which is the Atmospheric General Circulation Model (developed at CNRM), OPA8.1 ocean model (IPSL/LOCEAN, Paris,

France), GELATO2 dynamic and thermodynamic sea ice model (CNRM; Salas-Mélia 2002) and TRIP river routing scheme (University of Tokyo, Japan). These models are coupled together with OASIS2.2 (CERFACS). The version used in Stream 1 (CNRM-CM3.1) was based on the ARPEGE-Climat model version 3 described in Déqué et al (1994) and Gibelin and Déqué (2003). The model is based on the spectral method, the truncation used was a triangular T63 truncation with transformations to an associated linear Gaussian grid of 64x128 points (about 2.8° resolution) to compute the nonlinear terms and the physics. The vertical levels are defined with a progressive hybrid sigma-pressure vertical coordinate including 45 layers, 15 of them describing the stratosphere. The advection scheme is semi-Lagrangian, and the time integration is semi-implicit, with a 30 minute timestep, except for the radiative transfer (3 hour timestep). The physical parameterizations are similar to those used in previous versions of the ARPEGE-Climat model. OPA and Gelato share the same bipolar grid. This grid has a resolution of 2° in longitude and about 1° in latitude. The hydrological network of TRIP has a resolution of 1°. A detailed description of CNRM-CM3 model and simulations is given in Salas-Mélia et al (2005).

The standard GHG forcings defined for stream 1 where used, except the ozone concentration which is computed and transported by the ARPEGE-Climat model as a prognostic variable with a simplified parameterization of sources and sinks (Cariolle et al. 1990). For the sulphate aerosols only the direct radiative effect was taken into account. In the simulation including the natural forcings the effect of volcanic eruptions has to be taken into account indirectly by using the modified solar luminosity series adjusted to represent the absorption by volcanic aerosols. The land surface properties were kept fixed in all the simulations with values specified from the ECOCLIMAP land surface database (Champeaux et al. 2005).

For the stream 2 simulations an improved and updated version (CNRM-CM3.3) was used. In this version a new dynamical core based on ARPEGE-Climat version 4 has been used, and the whole system has been ported on a NEC-SX8 computer. The horizontal resolution is the same as in the stream 1 version, but it has been necessary because of computational constraints to reduce the vertical resolution from 45 to 31 levels. The coupling through OASIS has been revised in order to insure a better conservation of the energy fluxes through the interpolations between the atmospheric and oceanic grids. The ocean and sea-ice models have been checked carefully, and minor corrections have been made to improve the energy conservation. Improvements in the conservativity of the coupled system have allowed for reducing the drift in ocean volumetric and surface temperature and atmosphere 2m temperature. The global mean negative temperature bias has been much reduced between stream 1 and stream 2 (from 0.7°C to 0.1°C), but regional biases are slightly enhanced. The forcings defined for stream 2 have been taken into account except ozone that is computed and transported by the model. The linear system for ozone has been also modified to improve the simulation of the effects of chlorine on the ozone destruction. The indirect effect of sulphate aerosols has been introduced based on the parameterization of Boucher and Lohman (1995) with a calibration from POLDER satellite data given by Quaas and Boucher (2005). Finally the effect of stratospheric volcanic aerosols has been taken explicitly into account by introducing a new category of stratospheric aerosols. The changes in land use have been introduced through a modification of the fractions of crop and pasture types in the land-surface classification, and the resulting surface properties have been computed with an updated version (ECOCLIMAP-2) of the vegetation map.)

NERSC: BCM2 and BCM2-C model

The BCM2 coupled general circulation model is an updated version of the original BCM described in Furevik et al. (2003), which was used for IPCC AR4. The atmospheric part is ARPEGE-Climat3, which is based on the atmospheric GCM developed at METEO-FRANCE (Deque et al. 1994). In the version used for the ENSEMBLES project ARPEGE is run with a truncation at wave number 63 (TL63), and a time step of 1800 s. All the physics and the treatment of model nonlinear terms require spectral transforms to a Gaussian grid. This grid (about 2.8 deg resolution in longitude and latitude) is reduced near the poles to give an approximately uniform horizontal resolution (on the target sphere) and to save computational time. The vertical hybrid coordinate follows the topography in the lower troposphere, but becomes gradually parallel to pressure surfaces with increasing height. A total of 31 vertical levels are employed, ranging from the surface to 0.01 hPa. The physical parameterizations are similar to those used in previous versions of the model (Furevik et al. 2003). One exception is the vertical diffusion scheme, which has been updated to that of ARPEGE4. In the original version of the scheme a feedback could be activated in the case of a very cold surface. A cooling surface involved an increase in the stability, which in turn would prevent any heating by the atmosphere. This would accelerate the cooling until reaching a radiative balance, which could be very cold in the polar night. This phenomenon led to a significant cold bias in the global temperature in the IPCC version of BCM. To avoid the phenomenon a limitation has been added to the Richardson number in the new scheme.
The oceanic part is MICOM (Bleck and Smith 1990; Bleck et al. 1992), an isopycnic ocean GCM heavily modified at NERSC. Several important aspects deviate from earlier versions of the model (Furevik et al. 2003). Firstly, MICOM now uses a reference pressure of 2000 db whereas previous versions used a reference pressure of 0 db. This will reduce the non-neutrality of the isopycnals in the world ocean compared to having the reference pressure at the surface (McDougall and Jackett 2005). Secondly, the conservation properties of tracers (i.e. salinity, potential temperature and passive tracers) have been greatly improved compared to earlier versions. The use of incremental remapping (Dukowicz and Baumgardner 2000) for the advection of tracers has contributed to this. As a result of this model drift is greatly reduced, and the model can be run without flux adjustments. Thirdly, shear instability and gravity current mixing have been incorporated by adding a Richardson number dependent diffusivity to the background diffusivity. This has greatly improved the water mass characteristics downstream of overflow regions. Finally, the pressure gradient formulation used in the new version of MICOM is based on the formulation of Janic (1977), where the pressure gradient is expressed as a gradient of the geopotential on a pressure surface. This allows a more accurate representation of density in the pressure gradient formulation compare to earlier versions of MICOM. With the exception of the equatorial region, the ocean grid is almost regular with horizontal grid spacing approximately 2.4 deg $\times$ 2.4 deg. In order to better resolve the dynamics near the equator, the horizontal spacing in the meridional direction is gradually decreased to 0.8 deg along the equator. The model has a stack of 34 isopycnic layers in the vertical, with potential densities ranging from 1029.514 to 1037.800 kg m^{-3}, and a non-isopycnic surface mixed layer on top providing the linkage between the atmospheric forcing and the ocean interior.

There are currently two dynamic and thermodynamic sea-ice modules available for BCM2, both of which are handled as subroutine calls from MICOM. The first option is the sea-ice model developed at Nansen Environmental and Remote Sensing Center (NERSC). This model consists of one ice and one snow layer assuming a linear temperature profile in each layer, and the thermodynamics follows Drange and Simonsen (1996). The dynamic part of the model is based on the viscous-plastic rheology of Hibler (1979) with the modifications and implementation of Harder (1996). In addition, a multi-category sea-ice model, GELATO (Salas-Melia 2002), can also be

selected as the sea-ice component. GELATO uses an Arakawa B-grid, which shares its grid points with the C-grid of the ocean model. The sea-ice model performs a linear interpolation between the two grids internally. The different components are coupled together using OASIS2.2 (Terray and Thual 1995; Terray et al. 1995).

Recently, the Bergen earth system model (BCM-C) has been developed by coupling terrestrial and oceanic carbon cycle models into BCM2. The BCM-C adopts the Hamburg Ocean Carbon Cycle (HAMOCC5.1) model, which is based on the original work by Maier-Reimer (1993) with the extensions of Maier-Raimer et al. (2005). The model contains over 30 biogeochemical tracers, which include dissolved inorganic carbon, total alkalinity, oxygen, nitrate, phosphate, silicate, iron, phytoplankton, and zooplankton. For the terrestrial part BCM-C uses the Lund-Postdam-Jena Model (LPJ; Sitch et al. 2003), a large-scale terrestrial carbon cycle model, which includes global dynamical vegetation.

For the Stream 2 simulations two different versions of BCM have been used:

- The first version (BCM2) uses the GELATO sea ice model and has no carbon cycle included. A description and validation of a multi-century simulation for pre-industrial using BCM2 is given in Otterå et al. (2009a).
- The BCM-C version uses the original NERSC sea ice model and includes a full carbon cycle. The implementation of the vegetation and biogeochemistry into BCM2, and an assessment of regional climate-carbon-cycle feedbacks in this model have been made by Tjiputra et al. (2009).

The standard GHG forcings defined for stream 1 have been used for the historical and scenario simulations. The tropospheric sulphate aerosol forcing fields are based on the data set prepared for the stream2 (Boucher and Pham, 2002). Only the direct effect is currently taken into account in BCM. Unfortunately, the ozone and land-use forcings have not yet been implemented into BCM2 and BCM-C. The historical simulation of the BCM2 version also includes natural forcing due to solar and volcanic aerosol variations (Otterå et al. 2009b). This solar forcing differs somewhat from the default Stream2 data set, and is based on the Crowley et al. (2003) data set. The volcanic aerosol forcing time series (Crowley et al. 2003) include the monthly optical depths at 0.55 microns in the middle of the visible spectrum in four equal-area bands (90N-30N, 30N-equator, equator-30S and 30S-90S). The aerosol loading was distributed in each model level in the stratosphere, and the volcanic mass of the stratospheric aerosols were then calculated at each grid-point and model level in the stratosphere by dividing the total aerosol concentration by the total air mass of all stratospheric levels at that grid point. The model is able to successfully simulate many observed features after large tropical eruptions, such as the characteristic NH winter warming response (Otterå 2008).

4 The forcing and driving inputs

4.1 Stream 1

The Stream 1 and Stream 2 simulations make use of the methodology and the forcings that were defined for the CMIP3 (coupled Climate Model Intercomparison Project 3) simulations contributing to the IPCC AR4 assessment (http://www-pcmdi.llnl.gov/ipcc/about_ipcc.php).

Efforts have been made to implement the forcings in a similar way across the various models. In particular all the models used the same concentrations of the well-mixed greenhouse gases, even the models with carbon cycle are driven with the concentration of CO2, following the experimental design of Hibbard et al. (2007), which has been applied in stream 2 both to the pre-industrial control and to the historical 20C3M simulation. A first milestone (M2A.2) was to select a common set of anthropogenic and natural forcings, consistent with the forcings recommended in the CMIP3 project, and to use these forcings to drive a first set (Stream 1) of 20th Century ensemble simulations using existing coupled ocean-atmosphere climate models. The chosen natural forcings were the time series of solar irradiance of Solanki and Krivova (2003), and for the volcanic forcing an updated version of Sato et al. (1993). Some partners prefer to use the volcanic forcing as a simple modification of the solar constant (CNRM-CM3, IPSL-CM4).

For ozone and aerosol concentrations (as opposed to precursor emissions) some additional off-line chemical-transport modelling work has been required to generate the forcing datasets, via the University of Oslo-CTM2 troposphere-stratosphere GCM (Sovde et al. 2008) to derive ozone concentrations, and O. Boucher's transport model to derive the aerosol concentrations, both being driven by the necessary emissions (and climate) for given time slices, with interpolation between the time slices. The global land use/land cover change dataset (for crops and pasture) with 0.5°x0.5° resolution from 1700 to 2100 has been constructed and extrapolated for the scenarios taking into account historical reconstruction sources and the IMAGE model outputs. However, some extra model-specific processing has been required to blend this with the assumed undisturbed vegetation map, which differs between models.

However, due to specific limitations and constraints in certain models some differences in the implementations of the forcings still remain. The ozone 3-D concentration has been specified in the scenarios from the simulation provided by the UiO database, except IPSL-CM4 that used a fixed ozone concentration throughout all its simulations, INGV which used the data of Kiel et al. (1999), and CNRM-CM3.3 in which the ozone is a prognostic variable. For aerosols all models use the concentrations provided by O. Boucher, except HadGEM2-AO, HadCM3-C and EGMAM+ that have their own aerosol transport schemes.

Land-use changes were taken into account for stream 2 simulations in most models according to the specified land-use fractions, except in HadCM3-C, INGV, and BCM2-C in which land-use changes were not implemented. The volcanic forcing was represented in one of the 20CM3 simulations either by introducing a stratospheric aerosol layer, or by a change of the solar constant representing the radiative effect on the sulphate layer (IPSL-CM4, CNRM-CM3)

4.2 Stream 2

These are the same forcing fields as used in the Stream 1 IPCC simulations. For the core “Stream 2” simulations only anthropogenic forcings, i.e. without the solar and volcanic forcings, have been used. The difference from Stream 1 is the inclusion of the land-use changes. The dataset for the land use has been produced by Nathalie de Noblet over the period 1740-1992 for the LUCID project, based on crop dataset of Ramankutty and Foley (1999), and pasture from the HYDE dataset (Klein Goldewijk 2001) combined to give a fraction of grid-cell covered by crop and pasture on a 0.5x0.5° global grid for each year. The recommended methodology followed by the modelling groups was that each model keeps its standard vegetation map as used in Stream 1 simulations, and change only the crop and pasture fraction as provided in this dataset.

In the INGV model the ozone distribution from 1860 to 2100 is based on Kiehl et al. (1999). No land use changes were prescribed and/or considered.

A key part of the experimental design is that the subset of models that include the carbon cycle will diagnose the net flux of carbon into the atmosphere needed to achieve the prescribed (observed) concentration evolution, following the proposal of Hibbard et al. (2007), applied also to the pre-industrial control and to the historical 20C3M simulation. In turn, this will yield carbon emissions, with an ensemble spread as the results from any given model will depend on its carbon cycle formulation plus the feedback processes that govern the regional transient climate change for a given applied climate forcing.
The historical simulations (20C) use starting conditions from pre-industrial equilibrium runs (representing 1860 conditions) and are subsequently forced by the 20th century anthropogenic green house gas concentrations. All partners have run at least one realization of the simulation with greenhouse and aerosol (GA) forcings as in stream one, but with the improved model versions.

5 Key results from Stream 1

5.1: Runs completed and data availability

The different number of simulations are summarized in Table 4

Multimodel composition		Added components			1860-2000 simulations		
Partners	Model	LU	CC	AT	GA	GASV	Other
METO-HC	HadGEM1	●	●		3 **[3]**	3 **[3]**	2
METO-HC	HadCM3						
IPSL	IPSL-CM4				1 **[1]**	1	1
MPIMET +DMI	ECHAM5-MPI-OM				4 **[4]**	3	3
INGV	SINTEX-G				1 **[1]**		
FUB	EGMAM				3 **[3]**	1	1
CNRM	CMRM-CM3				1 **[1]**	1 **[1]**	
NERSC	BCCR-BCM2.0				1 **[1]**	1	

Table 4: *Multimodel simulations performed in ENSEMBLES Stream 1. The figures in the columns represent the number of simulations performed. The bold figures in the square brackets the number from these simulations that are available form the CERA database. GA represents the simulation with only anthropogenic forcings (Greenhouse gases and Aerosols) and GASV the simulations with anthropogenic and natural forcings (Solar and Volcanic).*

Due to the complex behaviour of the coupled atmosphere-ocean system one cannot expect climate models to reproduce all observed features, particularly at regional scales. As discussed in the IPCC report and elsewhere it does not make much sense to compare the detailed temporal evolution on regional or local scales of the surface temperature.
In order to synthesize the result we will show only the time evolution of global mean quantities.
Figure 1 illustrate the evolution of the annual global mean temperature at 2 m height in the different models. For model with multiple runs only a single simulation has been shown in order not to overburden the figure.

For comparison with the observed climate the global mean temperature computed in ERA40 reanalyses has also been shown. It can be seen that compared to ERA40 only the INGV-SX model has a warm bias, ECHAM5 and EGMAM have nearly no bias, while the other models have increasingly cold biases (HadCM3, CNRM-CM3, IPSL-CM4, HadGEM1 and BCM2). The interannual variability in the models is comparable to the interannual variability in the ERA40 reanalyses. All models display a warming trend over the 20th century, which tends to accelerate in the last 2 or 3 decades. The magnitude of the trend is in rather good agreement with the ERA40 data in the last decades, but varies more markedly between the models in the previous decades.

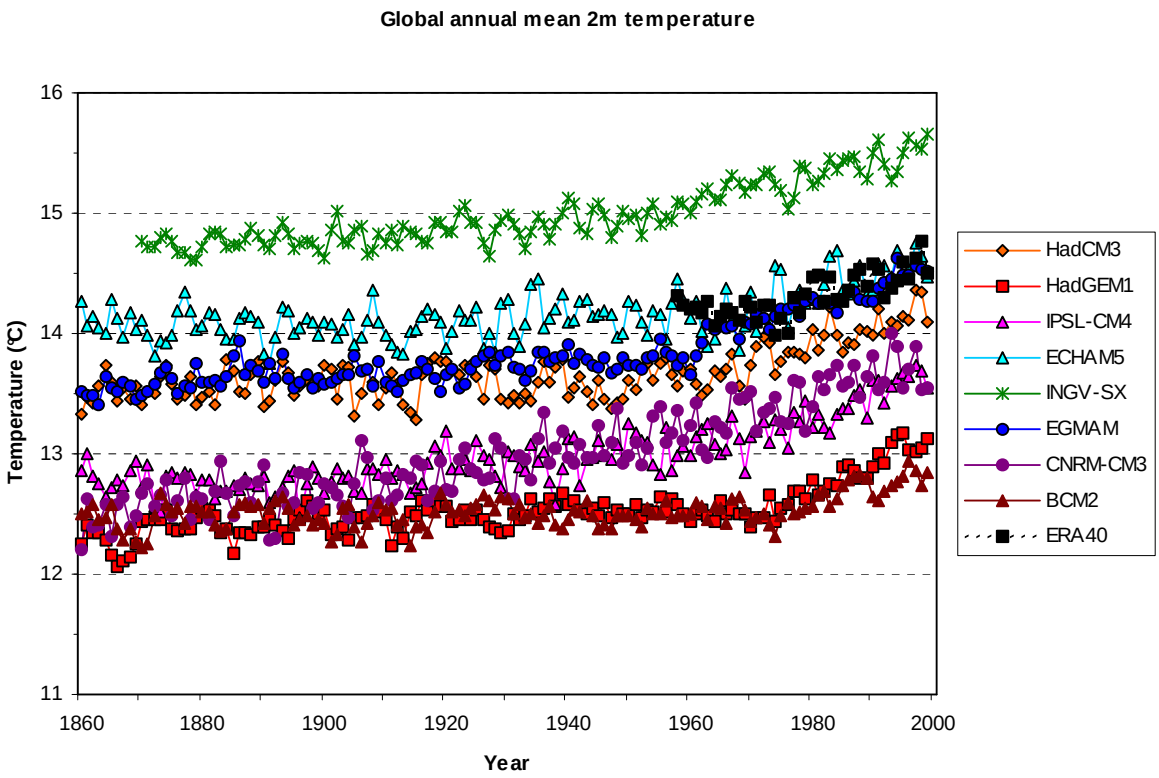

Figure 1: *Global annual mean temperature series in Stream 1 anthropogenic (GA) simulations. (For models with multiple runs only the first simulation has been plotted). The temperature from ERA-40 reanalysis has been plotted for comparison over the last 4 decades.*

The global mean precipitation (Fig. 2) vary rather strongly between the models, from about 2.6 mm/day for IPSL-CM4 to 3.2 mm/day in CNRM-CM3, with 3 models with similar precipitation of about 2.9 mm/day (ECHAM5, HadCM3, EGMAM). The ERA40 precipitation increases from about 2.9 mm/day in 1960 to more than 3.4 mm/day in 2000 with very large interannual fluctuations. In comparison the global annual precipitation series show in most models only a small and gradual increase of precipitation toward the end of the 20th century with some interannual variability. When compared to other global observed precipitation series such as CAMSOPI and GPCP, the interannual variability and trends in the ERA40 precipitation appear excessive. Since actually ERA40 is only an indirect diagnostic in the reanalysis the ERA40 rainfall cannot be used as a reliable source of information. The CAMSOPI and GPCP series are of too short duration (only 20 years) to allow a robust estimation of observed trends in global precipitation. The increase in precipitation in the models seems more or less parallel to the temperature increase, except for HadGEM1 and BCM2 which show rather constant values of precipitation throughout the 20th century.

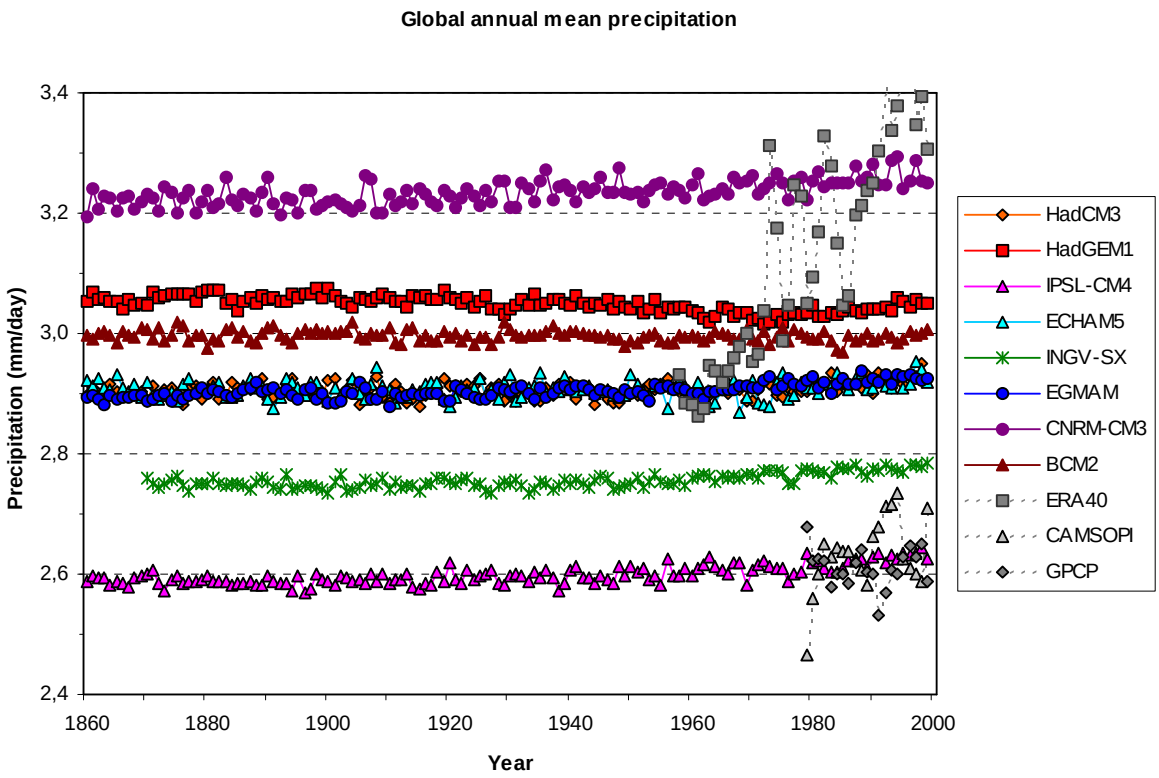

Figure 2: *Global annual mean precipitation series in Stream 1 anthropogenic (GA) simulations. (For models with multiple runs only the first simulation has been plotted). Precipitation estimates originating from ERA-40 reanalysis, CASOPI and GPCP have been plotted for comparison.*

The increase of precipitation seems for most models linearly correlated to the temperature increase.linearly related to temperature increase as can be seem from a scatter diagram of precipitation versus temperature anomaly (figure 3). Exception to this relationship are the HadGEM1, HadGEM2, and BCM2 simulations in which the global precipitation remain rather stable throughout the 20th century, while other models have a similar linear precipitation/temperature relationship.

6 Key results from Stream 2

As explained in paragraph 3 the models used for ES2 simulations are improved and extended versions of those used in Stream 1. Table 5 provides a summary view of the models used and simulations performed with them. Land use forcing has been introduced into 5 models (HadGEM2-AO, IPSL-CM4, ECHAM5, EGMAM+, CNRM-CM3), carbon cycle components into 5 models (HadCM3C, IPSL-LOOP, ECHAM5, C-ESM, BCM-C), and aerosol transport into 3 models (HadGEM2-AO, HadCM3C, EGMAM+). All the models have performed the simulation with anthropic forcings only (greenhouse gases and aerosols, and land use for those that include this forcing). The simulation with forcings (solar and volcanic) has been performed with 4 different models (together with anthropic forcings for IPSL-CM4, EGMAM+, CMRM-CM3, and without it for BCM2). A few complementary simulations with different combinations of the forcings have been performed by some models and are entered in column "other". Some of the models where able to perform small ensembles of simulations (IPSL-CM4, ECHAM5 and CNRM-CM3 with the help from DMI) so has to enlarge the number of available simulations (the figure in the columns indicate the number of simulations). The identifiers that have been used to designate the different models in the legend of subsequent figures are provided in the last column of table 5.

Multimodel composition		Added components			1860-2000 simulations			Identifier
Partners	Model name	LU	CC	AT	GA (+LU)	GA+SV (+LU)	Other	N° used in figures
METO-HC	HadGEM2-AO	●		●	1			1a
METO-HC	HadCM3C		●	●	1			1b
IPSL	IPSL-CM4 IPSL-LOOP	●	 ●		3 1	3	1: GA+SV	2a
MPIMET +DMI	ECHAM5-C	●	●		3 3			3 4
FUB	EGMAM+	●		●	2	2	1: SV+LU	5
INGV	C-ESM		●		1			6
CNRM + DMI	CMRM-CM3.3	●			1 2	1		7 8
NERSC	BCM2 S1 BCM2 S2 BCM-C		 ●		1 1 1		 1: SV	9a 9b 9c

Table 5: Multimodel Stream 2 global simulations (number of simulations). ENSEMBLES Stream 2 multi-model summary (CC = carbon cycle component; AT = aerosol transport/chemistry component; LU = transient land use forcing), and simulations performed with results included in this paper (GA = historical forcing by GHGs and aerosols, plus land use change if represented; +SV = plus solar and volcanic forcing. ● = model component included/simulations (or ensemble of **N**) completed. The identifiers in the last column are used for model identification in the legend of the following figures

In order to illustrate at a glance the changes between the versions of the models used in stream 1 and stream 2 annual mean global precipitation and temperature series have been displayed in a scatter diagram (Figure 3).

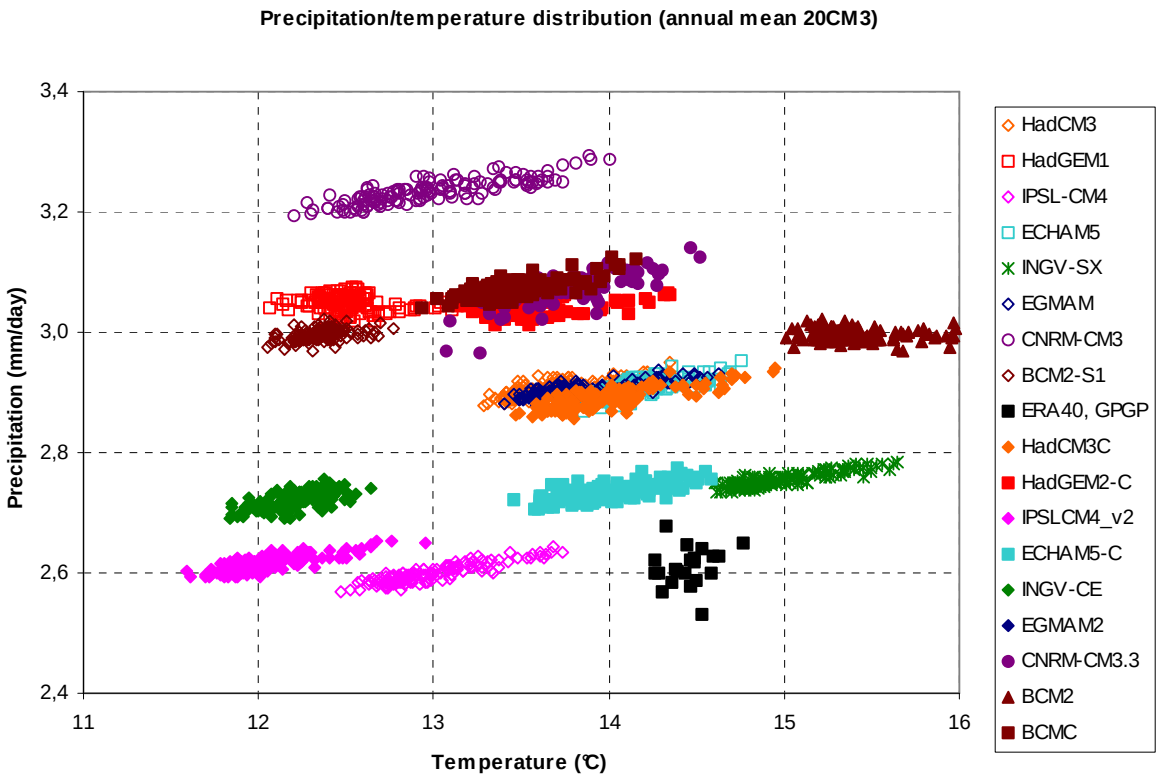

Figure 3: *Global annual mean precipitation versus temperature distribution in the Stream 1 (hollow symbols) and Stream 2 simulations (filled symbols).*

Detailed examination of this scatter diagram shows that generally the model biases are different in the stream 2 and stream 1 versions. For comparison with observations we have used ERA40 for global temperature and GPCP for global precipitation. For several models the biases have been somewhat improved in stream 2. For example the cold biases in HadGEM1, CNRM-CM3 and BCM2-S1 have been reduced in HadGEM2, CNRM-CM3.3 and BCM-C. The excessive precipitation in CMRM-CM3 have been reduced, and those of ECHAM5-C have become closer to GPCP observations. However there are models for which the introduction of supplementary components have resulted in a strengthening of the biases (increase of the cold bias in IPSLCM4-v2, replacement of a warm bias in INGV-SX by a cold bias in INGV-CE, positive bias in BCM2).

Further analysis of the annual time-series in stream 2 has been made to compare the simulations first without natural forcings. Fig. 4 shows time-series of the globally averaged annual mean near-surface temperature over the period 1861-2000 based on the 12 hindcasts in GA and GA+LU. In those cases, where ensembles of simulations, are available the ensemble mean values are shown. This figure shows that the models generally fall into three categories, with one model showing a

marked positive temperature bias and three models marked negative biases. Most models show temperatures between 13 and 14 ºC at the beginning of the period considered. All models show a warming over the second half of the 20th century, in agreement with stream one simulations.

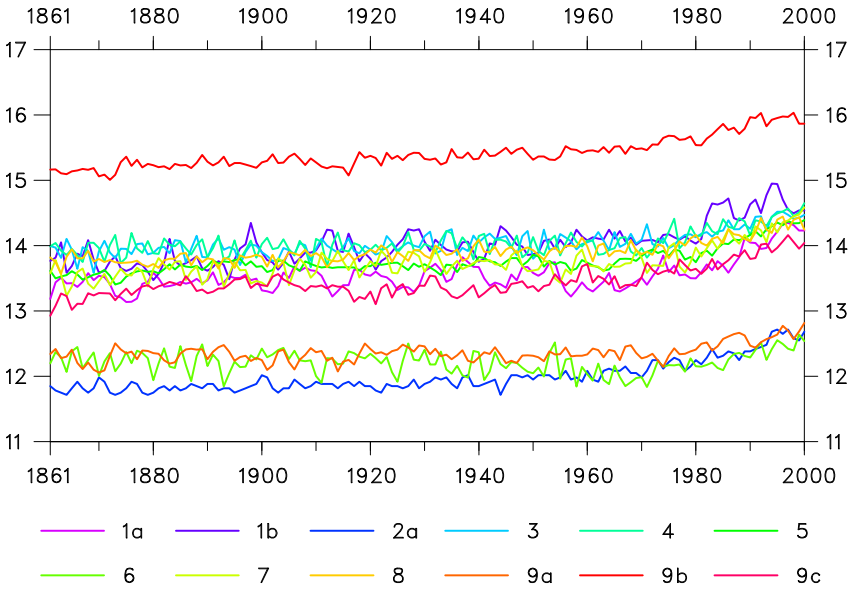

Figure 4: *Time series of the globally averaged annual mean near-surface temperature over the period 1861-2000 for the 12 hindcasts in GA and GA+LU. The numbers indicating the different models/simulations are taken from the preceding table. Units are [ºC].*

In order to highlight more clearly the warming trend in the simulations, it is useful to remove the model biases from the time series. This can be done quite easily by computing for each model the anomalies with respect to a chosen reference period. We have chosen to use the average over 1861-1890 as reference period in the following figures, in order to show clearly the changes over the 20th century. We have also computed a multi-model average of the annual anomalies in order to highlight the common features appearing in the simulations.

When the potential biases are removed, most models show a marked warming over the last 30 years of the 20th century (Fig. 5). In only one of the hindcasts, on the other hand, the marked warming does not start before the mid-eighties. Though the individual models show some large differences at the end of the 20th century due to both there interannual variability and different trends, the multi-model ensemble mean is in rather good agreement with observations as concerns the overall trend over the period, though some transient decadal variability in the observations (cold decades between 1890-1920, warm decade around 1940) cannot obviously be reproduced by the models with only the anthropogenic forcings.

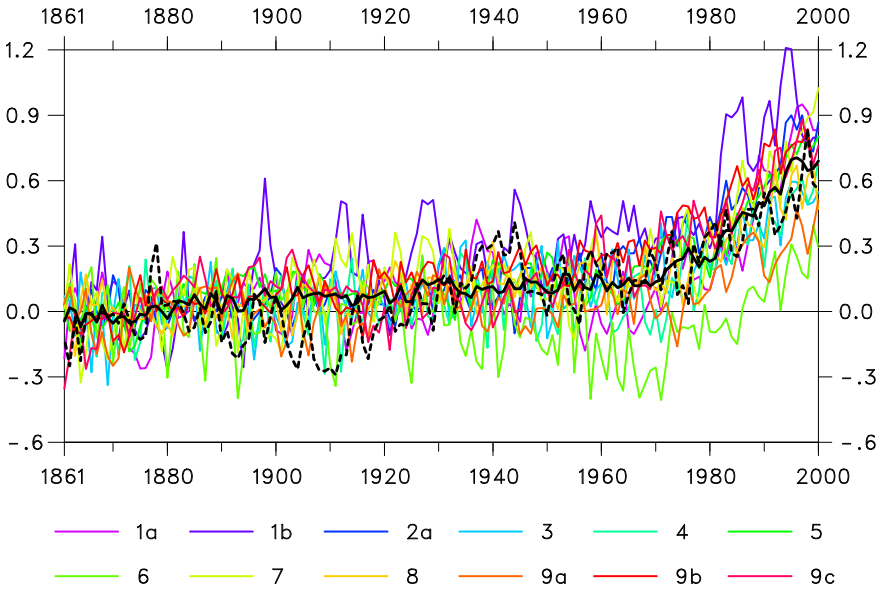

Figure 5: *Anomalies of the globally averaged annual mean near-surface temperature over the period 1861-2000 with respect to the period 1861-1890 for the 12 hindcasts in GA and GA+LU. The solid black curve indicates the multi-model mean values (giving equal weight to the different models) and the dashed black curve the observational values (HadCRUT3). The numbers indicating the different models/simulations are taken from the preceding table. Units are [ºC].*

In order to investigate the potential role of the natural forcings in explaining the observed variability we have produce a figure similar to figure 5 with all the simulations in which the solar and volcanic (SV) forcings were taken into account (figure 6)

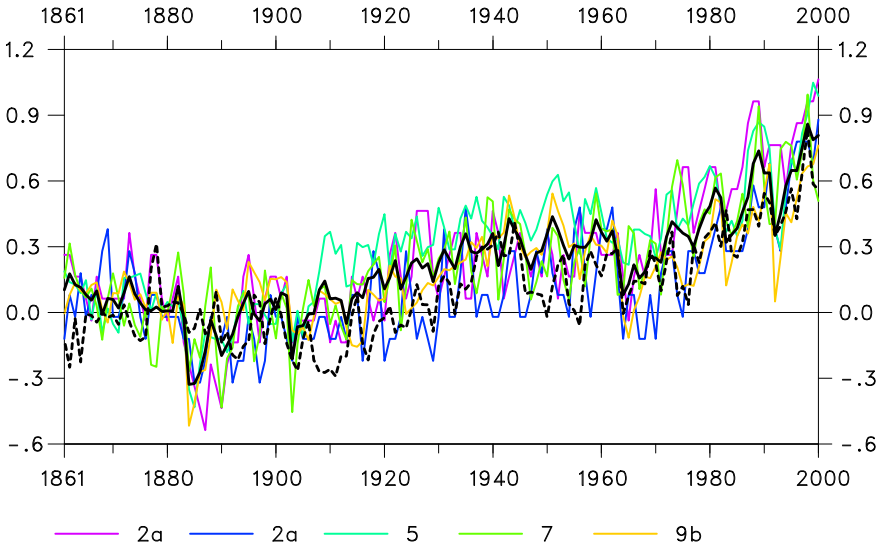

Figure 6: *As for Fig. 5 but for the 5 hindcasts in GA+SV and GA+LU+SV.*

Considering the historical forcing by solar variability and volcanoes in the model simulations generally increases the variability of the globally averaged temperatures. Particularly in the 1880's and in the last 40 years of the 20th century these forcing factors lead to a marked cooling of the global mean temperatures after major volcanic eruptions, which brings them in better agreement with observations than the simulations with only anthropogenic forcings shown in figure 5.
Examination of the two simulations without greenhouse gas and aerosol forcings (figure 7) confirms that the greenhouse and aerosol forcing is absolutely necessary to reproduce the warming trend of the last 3 decades of the 20th century.

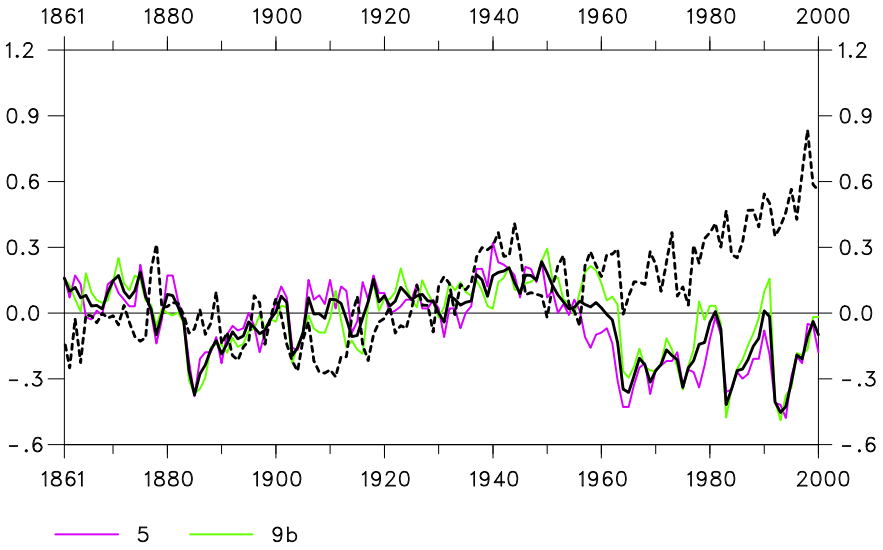

Figure 7: *As for Fig. 5 but for the 2 hindcasts in SV and LU+SV.*

In addition to the aforementioned abrupt cooling of the global mean temperatures, these hindcasts also reveal a general cooling trend over the last 40 years of the 20th century, masking the marked warming caused by the well-mixed greenhouse gases in this period.

The analysis is continued by examining the precipitation changes in the stream 2 simulations.
As in stream 1 simulations, for the globally averaged annual mean precipitation, the different models show large variations, ranging from about 2.6 mm/d for the driest to about 3.2 mm/d for the wettest model (Fig. 8). The driest and the wettest model are those with the strongest cold and warm temperature bias, respectively (see Fig.3 and fig. 4).
Applying the same methodology as for temperature a series of precipitation anomalies with reference to the 1861-1890 has been constructed to highlight the precipitation trends (Figure 9). However for precipitation there are no reliable observed time-series of sufficient duration to validate the model trends.
Most models show a marked increase in precipitation only over the last 20 years of the 20th century. But in contrast to the near-surface temperature, two of the hindcasts, are characterized by rather negative or weak precipitation trend during the second half of the 20th century. One of the models is also characterized by cooling in the 1960's and 1970's and a relatively weak warming during the last 20 years of the 20th century (see Fig. 5).

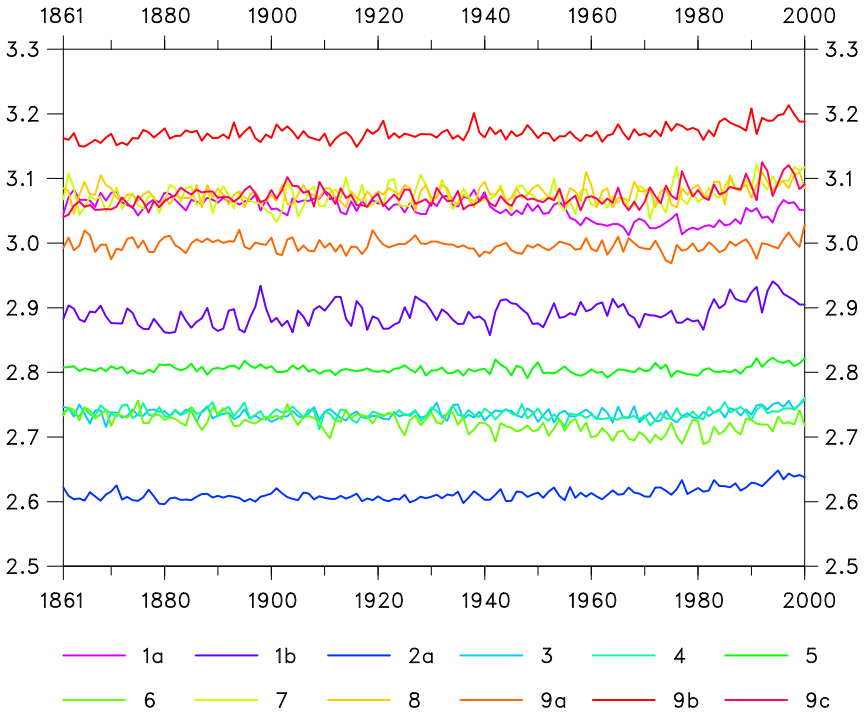

***Figure 8**: As for Fig. 4 but for precipitation intensity. Units are [mm/d].*

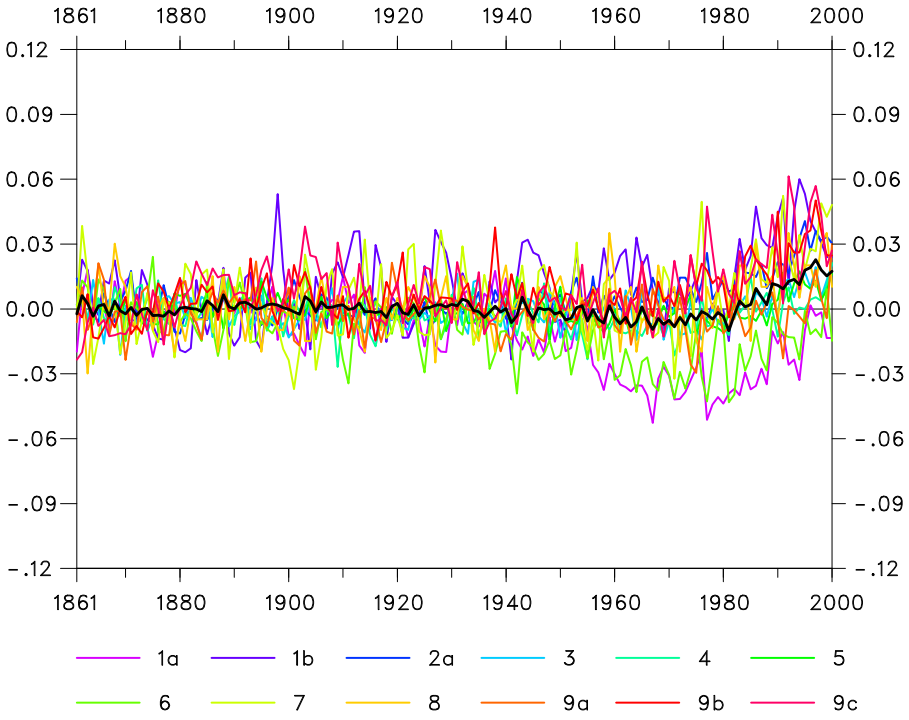

***Figure 9:** As for Fig. 5 but for precipitation intensity (no observational data are available). Units are [mm/day].*

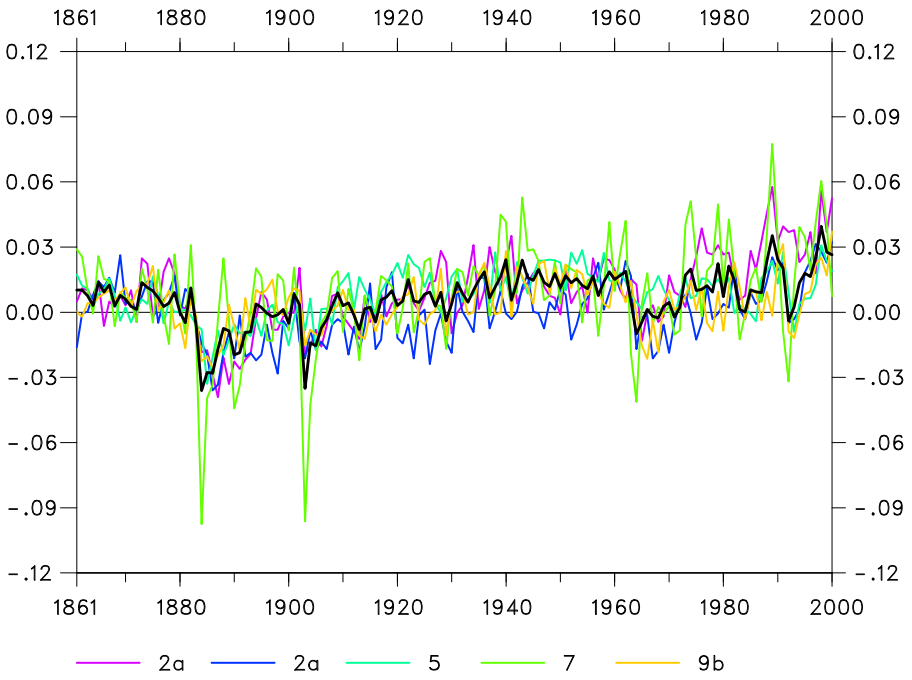

Figure 10: *As for Fig. 6 but for precipitation intensity (without observed data). Units are [mm/day].*

In correspondence with the near-surface temperature (see Fig. 6), the globally averaged precipitation is characterized by large variations in the 1880's and over the last 40 years of the 20th century (Fig. 10). In particular one model (7=CNRM-CM3.3) shows an excessively strong response to the SV natural forcing. Further analysis of this simulation has shown that the stratospheric absorption of volcanic aerosols was incorrectly specified in CNRM-3.3 and that this lead to unrealistic effect on precipitation response. The other model show more agreement in simulating a transient reduction in global precipitation following major volcanic events.

This can also be seen in Fig. 11, where the hindcasts not considering changes in the well-mixed greenhouse gases and in the sulphate aerosols are shown. In addition to the aforementioned abrupt reductions in the global mean precipitation, these hindcasts also reveal a general drying trend over the last 40 years of the 20th century, consistent with a corresponding cooling trend in these simulations (see Fig. 7)

The previous analysis has allowed to indentify the impact of the natural forcings, particularly the effect of major volcanic eruptions, on the interannual variability in the simulations. We will continue a more systematic analysis of the impact of volcanic forcing in the following paragraph.

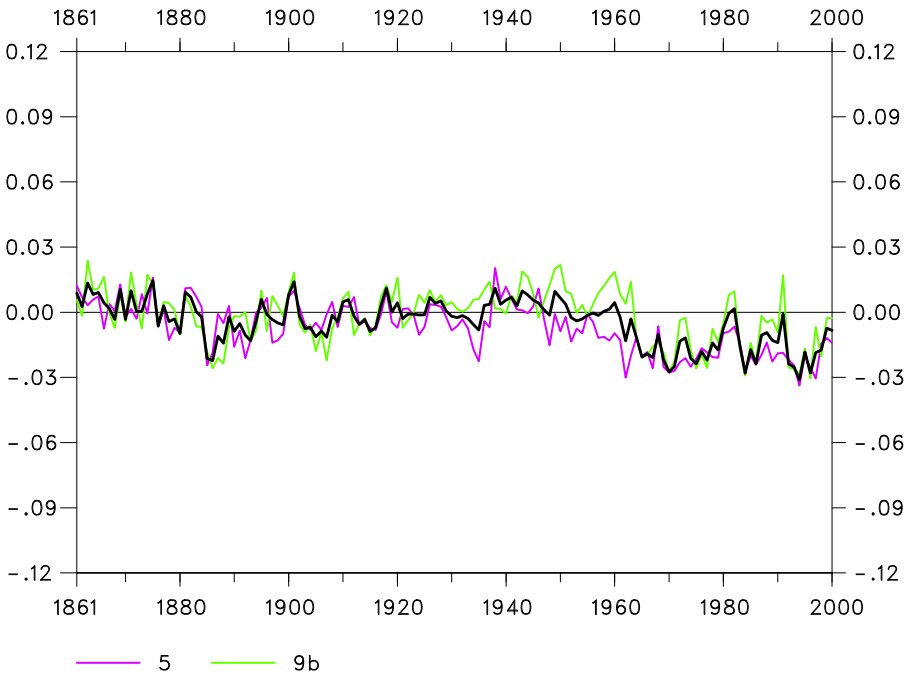

Figure 11: *As for Fig. 7 but for precipitation intensity and without considering any observational data. Units are [mm/d].*

7 Analysis of the role of the natural forcings

In this paragraph we will combine the stream 1 and stream 2 simulations with natural forcings (SV: solar and volcanic) in order to increase the sample available for an analysis of the impact of these forcings on the variability of the 20C3M simulations.

As a first analysis we have attempted to isolate the effect of the natural forcing by computing the difference between the simulations with the SV forcing and the simulations without SV forcing, for each model in which the two kinds of simulations have been performed. The simulations for stream 1 are those with HadGEM1, ECHAM5, CNRM-CM3, and those for stream 2 with IPSL-CM4, EGMAM2 (The CNRM-CM3.3 stream 2 simulation has not been taken into account due to the erroneous volcanic effect pointed out in the previous paragraph). To increase the size of the sample we have also added the stream 2 simulations which have been run without the greenhouse aerosol forcings from EGMAM2 (LU+SV simulation) and from BCM2 (SV simulation). For model with multiple runs (ECHAM5, IPSL-CM4) an average over the available simulations has been performed (in order to reduce the sampling fluctuations), before computing the difference between the simulations with and without the SV forcing.

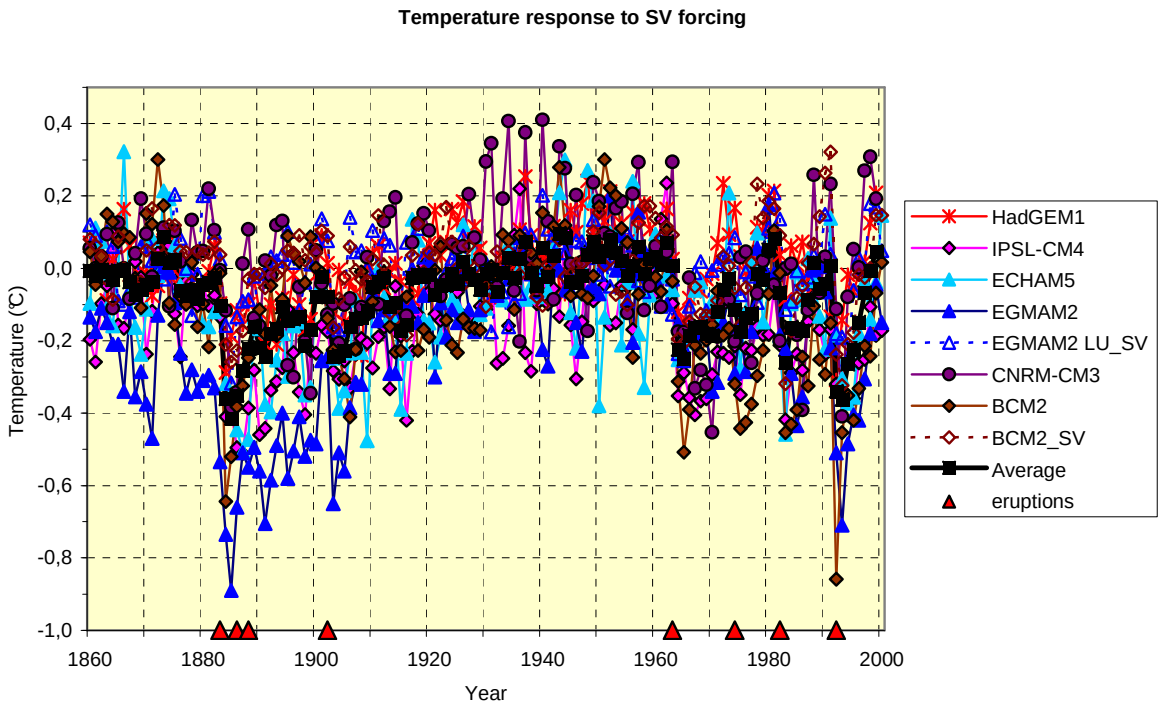

Figure 12: *Annual mean global temperature difference between the runs with and without natural forcing for the different models. The average over the models is represented as the thick black line and squares. The year of the major volcanic eruptions are indicated by a red triangle centred on the year of the eruption.*

The resulting time series from the different model and the multi-model average are shown in figure 12 for 2m temperature and figure 13 for precipitation. Though the model present large interannual variability (enhanced by taking the difference between the two series with and without SV forcing) it can be seen that there are several periods where strong transient negative anomalies appear, in particular in the years following major volcanic eruptions. The multi-model average shows that the magnitude of the temperature drop can reach of the order of 0.2 to 0.4 K.

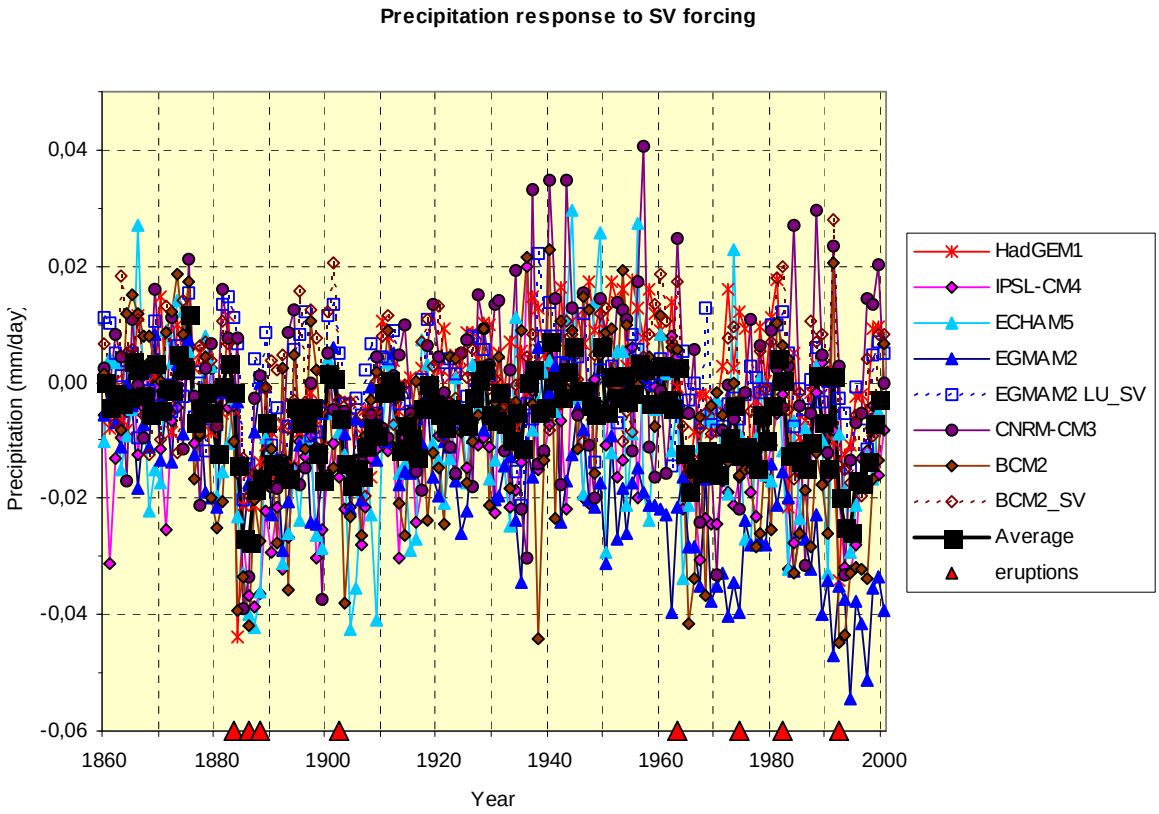

***Figure 13**: Annual mean global precipitation difference between the runs with and without natural forcing for the different models. The average over the models is represented as the thick black line and squares. The year of the major tropical volcanic eruptions are indicated by a red triangle centred on the year of the eruption. The name of the eruption, date and latitude can be found in table 6.*

The precipitation response (figure 13) is more noisy than the temperature response, but a systematic decrease of the order of 0.1 to 0.2 mm/day can be noticed in the years following the major volcanic explosions.

Using two time series to remove the effect of the long term trends due to increasing greenhouse aerosols forcings has the unfortunate effect of increasing the noise level by taking differences between the time series. We have therefore continued the analysis of the impact of volcanic eruption by applying a method based on the composite analysis on the series with SV forcings.

First we have selected the years with major low latitude volcanic eruptions as indicated in Table 6, based on the analysis of Stenchikov et al. (2006).

Figure 15 compares the resulting radiative effect of the major volcanic explosions listed in table 6 by showing the annual mean global radiative forcing anomalies according to Sato et al () in the 3 years before and the seven years after the eruption year (noted as year 0). This figure shows that the radiative impact is maximum in the year following the eruption and relaxes gradually towards zero in the 4 years following the eruption. Exceptions to this pattern are seen for the eruption of 1886 Tarawera in 1886 which is masked by the strong eruption of Krakatau 3 years before, and for the eruption of Bandai in 1888, where the influence of both former eruption is still prominent. The eruption of Quizapu in 1932 has only a very week influence probably due to the higher latitude of the eruption. As the patterns of the radiative forcing for these 3 eruptions are week and ill defined they have been removed from the following composite analysis.

Volcano name	Eruption date (JJ/MM/YYYY)	Latitude
Krakatau	27/08/1883	6.10 °S
Tarawera	10/06/1886	38.23 °S
Bandai	15/07/1888	37.60 °N
Santa Maria	24/10/1902	14.76 °N
Quizapu	10/04/1932	35.65 °S
Agung	17/03/1963	8.34 °S
Fuego	10/10/1974	14.47 °N
El Chichon	04/04/1982	17.36 °N
Pinatubo	15/06/1991	15.13 °N

Table 6*: Main characteristics of the major low-latitude volcanic eruptions used in Stenchikov et al (2006). The 3 eruptions overlayed in grey are not used in the compositing for the current study.*

The compositing has been done for the 8 model runs with a simulation with SV forcing, for each of the 6 selected years with well separated major volcanic eruptions (1883, 1902, 1963, 1974, 1982, 1991) using the eruption year as year 0. In order to remove the long term trends due to GA forcing in the simulations, and isolate the immediate impact of the eruption the compositing has been done with the model anomalies with respect to the year before the eruption (year –1). Other attempts where made for defining the anomaly with respect to a model average over a larger number of years around the eruption but the results were qualitatively very similar, and so the simpler method of using as a reference the single year before the eruption was preferred for producing the following illustrations.

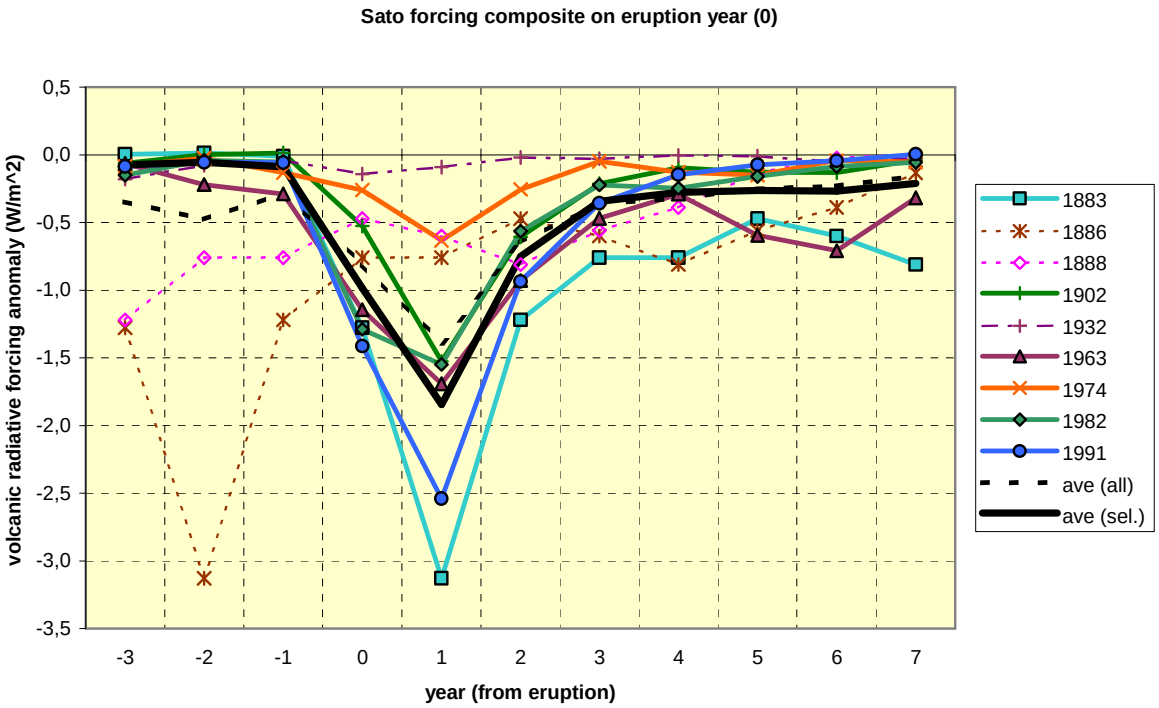

Figure 14: Composite of the volcanic radiative forcing anomaly (W/m2) computed from Sato data with respect to the eruption year (year 0) for the major volcanic eruptions in the period 1860-2000. The dotted black line represents the composite averaged over all the eruptions. The thick black line represents an average over the 6 selected eruption years (continuous lines) after discarding the non representative eruptions (dotted lines).

In order to filter the interannual fluctuation two averaging methods were applied:

- averaging over the 6 eruptions in order to show the differences between the models
- averaging over the 8 model runs in order to show the differences between the eruptions

The average composites, applied to global mean 2m temperature and global mean precipitation, are presented in the following figures.

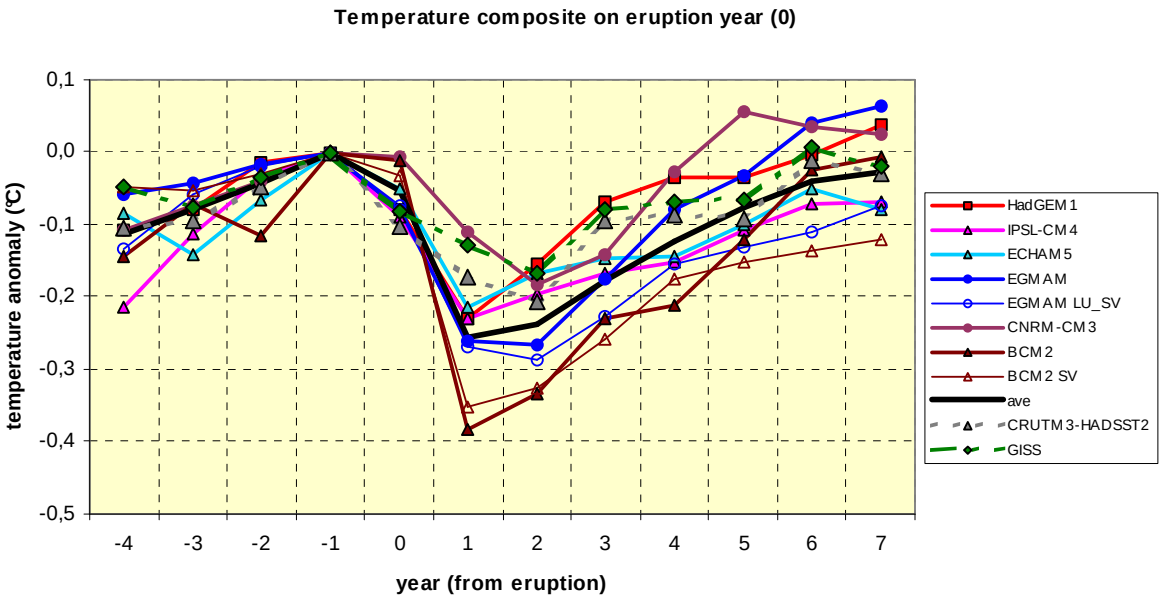

Figure 15: *Composite with respect of the eruption year (year 0) of the global annual mean temperature response for the different models and observations as averaged over the selected eruptions. The response is computed as a difference from the value in the year preceding the eruption (year –1). The results for the different models are shown as continuous colour lines. The black continuous line represents the average over the models. For comparison composites from two observed time series (CRUTM3-HADSST2 and GISS) are shown as dashed lines.*

The temperature response averaged over the 6 eruptions (figure 15) shows that the models have a similar pattern of response, but with different amplitudes. By construction the anomalies have a zero value in the year preceding the eruption (year –1). A negative anomaly starts to appear in the year of the eruption and reaches its peak value generally in year +1 after the eruption (HadGEM1, IPSL-CM4, ECHAM5, BCM2) or at year +2 (EGMAM, CNRM-CM3). Then the negative anomaly tends to return slowly to zero in the next few years. Most model have a very similar amplitude response (-0.2 to -0.25 K) in year +1, except BCM2 which has a stronger response (-0.35 to -0.4 K), and CNRM-CM3 for which the response (-0.1 K) intensifies further at year 2 (about –0.2 K). The pattern of the model responses is qualitatively in agreement with observations based on the GISS and CRUTM3-HADSST2 global mean temperature series, though the amplitude of the observed response is slightly weaker than the average model response.

Comparison of the mean model response (averaged over the 8 simulations) for the different eruptions (figure 16) shows that the amplitude of the temperature response is generally in agreement with the magnitude of the radiative forcings associated with the eruptions (figure 14).

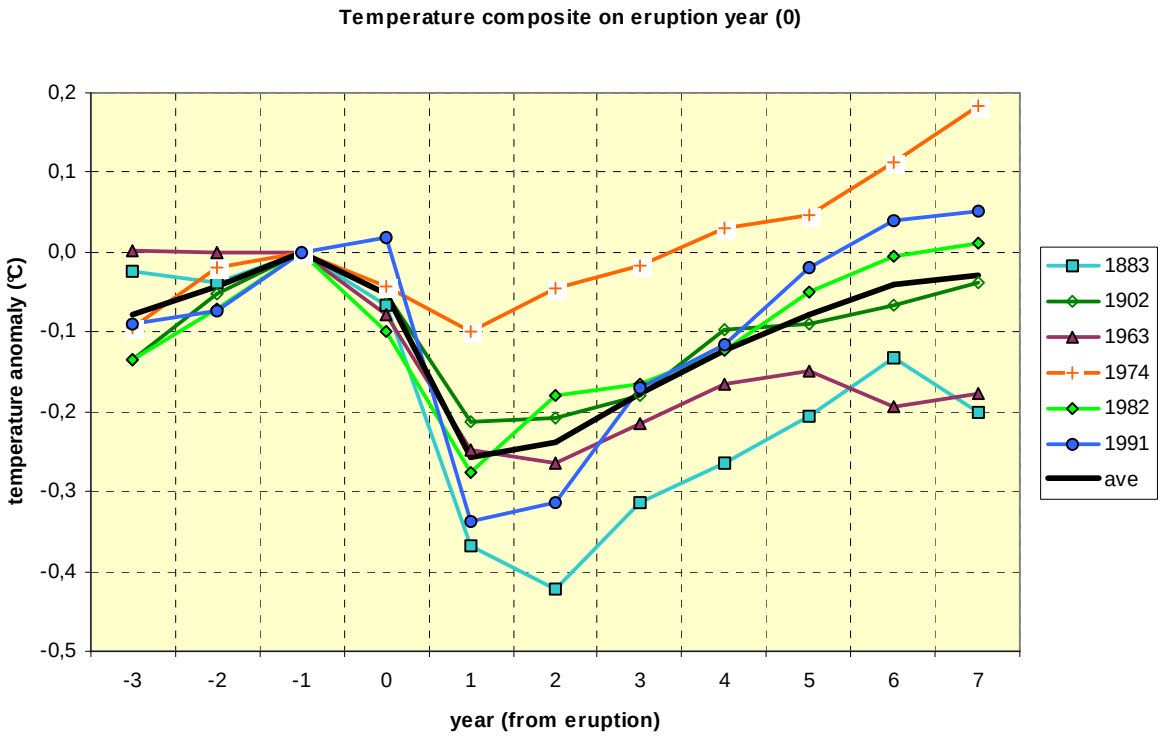

Figure 16: *Composite with respect of the eruption year (year 0) of the global annual mean temperature response averaged over the different models. The response is computed as a difference from the value in the year preceding the eruption (year –1). The results for the different eruptions are shown as continuous colour lines labelled with the year of the eruption. The black continuous line represents the average over all the eruptions.*

The stronger responses (more than –0.3 K cooling) are found for the two stronger eruptions (Kratkatau 1883, and Pinatubo 1991), and the weakest (barely –0.1 K) for the weakest eruption (Fuego 1974). The other 3 eruptions produce rather similar temperature responses with maxima between –0.2 and –0.3 K.

The composite of the global annual mean precipitation (figure 17) shows much larger differences in model responses than for the 2m temperature.

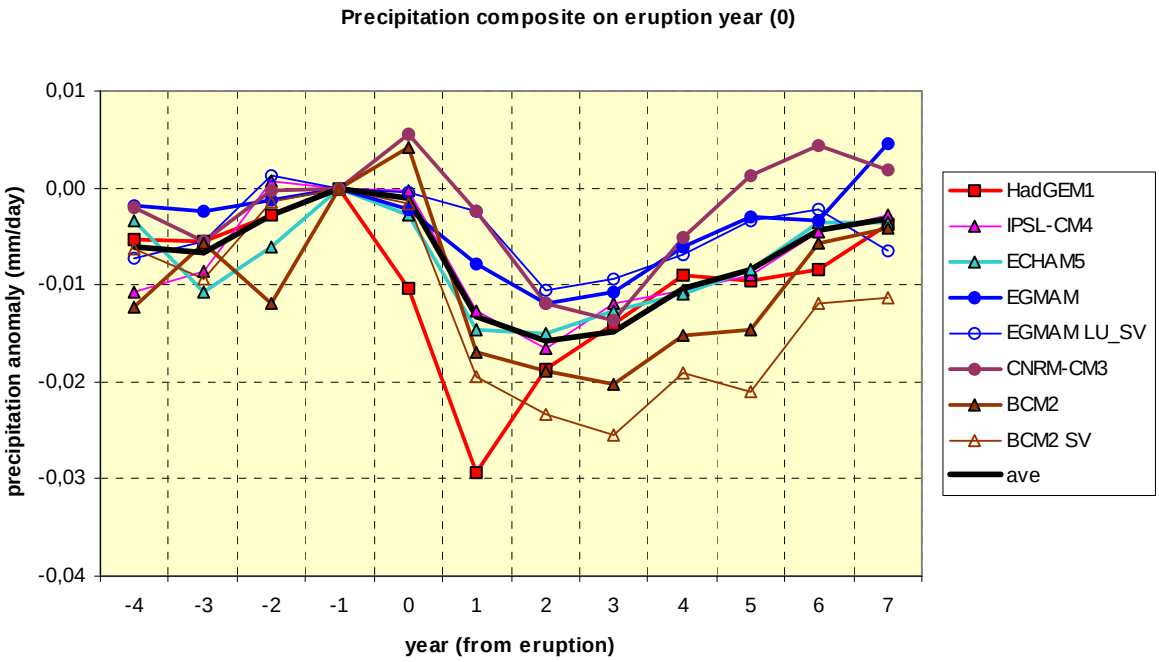

Figure 17: *Composite with respect of the eruption year (year 0) of the global annual mean precipitation response for the different models averaged over the selected eruptions. The response is computed as a difference from the value in the year preceding the eruption (year –1). The results for the different models are shown as continuous colour lines, the average over the models as a black continuous line.*

For most model the amplitude of the precipitation response corresponds to the temperature response (higher response for BCM2 and lower response for CNRM-CM3), except for HadGEM1 which has a very strong precipitation response at year 0 and +1. On average the maximum precipitation response seems to be delayed by about one year compared to the temperature response, and the maximum response occurs around year +2 and +3 with an average amplitude of about –0.015 mm/day.

The differences in the mean model response for the different eruptions (figure 18) are in good agreement with the temperature response to the strength of the volcanic forcing (figure 16). The precipitation response is very weak for the Fuego (1974) eruption, and very strong for the Krakatau (1883) eruption (reaching more than - 0.03 mm/day). For the other 4 eruptions the precipitation response is very similar with minima between –0.01 and –0.02 mm/day.

Conclusions of the analysis:

The use of 8 different simulations and 6 different volcanic eruptions allows to highly a coherent and robust response in global annual mean near surface temperature and precipitation to the radiative forcing perturbations caused by the volcanic aerosols. The transient response to volcanic eruption can reach a magnitude that is of the same order as the trends observed in the last decades of the 20th century. Thus it appears that volcanic forcing is an important factor to take into account in simulations aimed at explaining the interannual variability of the climate in the 20th century and for detection studies of the impact of anthropogenic perturbations.

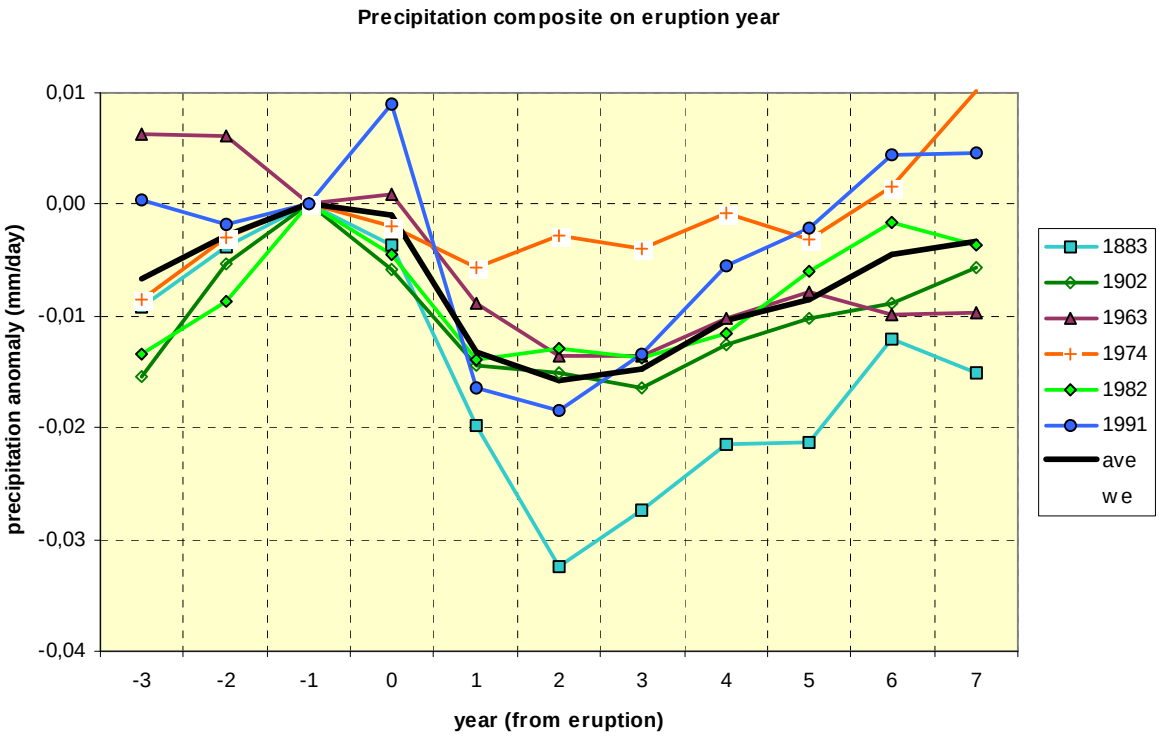

Figure 18: *As in figure 16 for the composite with respect of the eruption year (year 0) of the global annual mean precipitation response averaged over the different models.*

8 Data Accessibility

All Stream 1 and Stream 2 data are available from the CERA data base (http://cera-www.dkrz.de/CERA/) in Hamburg.

Data from the RT2A simulations for the historical period (20C3M) are archived in CF-compliant netcdf format. The data included cover monthly mean values, daily values (daily mean, max and min, or instantaneous, depending on the variable), and also several instantaneous variables at 6- and 12-hourly resolution at the surface and on vertical pressure levels. The multi-model dataset and associated metadata is accessible through the CERA portal (http://cera-www.dkrz.de) subject to user registration. Additional variables other than those archived at CERA may be available on request direct from the associated ENSEMBLES partners or from other data centres (contact details are given in the metadata).

References:

Alessandri, A (2006): Effects of Land Surface and Vegetation Processes on the Climate Simulated by an Atmospheric General Circulation Model. PhD Thesis in Geophysics, Bologna University Alma Mater Studiorum, 114 pp

Aumont O, Maier-Reimer E, Blain S, Monfray P (2003) An ecosystem model of the global ocean including Fe, Si, P colimitations. Global Biogeochem Cycles 17: 1-26

Bellouin, N., co-authors (2007) Improved representation of aerosols for HadGEM2. Hadley Centre Technical Note No. 73, Met Office, Exeter, UK, 42pp

Bleck R, Smith LT (1990) A wind-driven isopycnic coordinate model of the North and equatorial Atlantic Ocean. 1: model development and supporting experiments. J Geophys Res (Oceans) 95: 3273-3285

Bleck R, Rooth C, Hu D, Smith LT (1992) Salinity-driven thermocline transients in a wind- and thermohaline-forced isopycnic coordinate model of the North Atlantic. J Phys Oceanogr 22: 1486-1505

Booth BBB, Jones CD, Collins M, Totterdell IJ, Cox PM, Sitch S, Huntingford C, Betts RA, Harris GR (2009) Global warming uncertainties due to the land carbon cycle may exceed those due to socioeconomics (manuscript in preparation).

Boucher O, Lohmann U (1995) The sulfate-CCN-cloud albedo effect: A sensitivity study with two general circulation models. Tellus (Ser B) 47: 281-300

Boucher O, Pham M (2002) History of sulfate aerosol radiative forcings. Geophys Res Lett 29: doi: 10.1029/2001GL014048

Cadule, P., L. Bopp, and P. Friedlingstein, 2009: A revised estimate of the processes contributing to global warming due to climate-carbon feedback, Geophys. Res. Lett., 36, L14705, doi:10.1029/2009GL038681.

Cariolle D, Lasserre-Bigorry A, Royer JF, Geleyn JF (1990) A general circulation model simulation of the springtime Antarctic ozone decrease and its impact on mid-latitudes. J Geophys Res (Atmos) 95: 1883-1898

Champeaux JL, Masson V, Chauvin R (2005) ECOCLIMAP: A global database of land surface parameters at 1 km resolution. Meteorol Appl 12: 29-32

Collins M, Booth BBB, Harris GR, Murphy JM, Sexton DMH, Webb MJ (2006) Towards quantifying uncertainty in transient climate change. Clim Dyn 27: 127-147

Collins WJ, Bellouin N, Doutriaux-Boucher M, Gedney N, Hinton T, Jones CD, Liddicoat S, Martin G, O'Connor F, Rae J, Senior C, Totterdell I, Woodward S. Reichler T, Kim J (2008) Evaluation of the HadGEM2 model, Met Office Hadley Centre Technical Note No. 74, Met Office, Exeter, UK, 47 pp

Cox PM, Betts RA, Jones CD, Spall SA, Totterdell IJ (2000) Acceleration of global warming due to carbon-cycle feedbacks in a coupled climate model. Nature 408: 184-187

Crowley TJ, Baum SK, Kim KY, Hegerl GC, Hyde WT (2003) Modeling ocean heat content changes during the last millennium. Geophys Res Lett 30: doi: 10.1029/2003GL017801

Déqué M, Dreveton C, Braun A, Cariolle D (1994) The ARPEGE/IFS atmosphere model: A contribution to the French community climate modelling. Clim Dyn 10: 249-266

Drange H, Simonsen K (1996) Formulation and spin-up of the ESOP2 version of MICOM, Tech. Rep. 117, Nansen Environmental and Remote Sensing Center, Bergen, Norway

Dufresne JL, Quaas J, Boucher O, Denvil S, Fairhead L (2005) Contrasts in the effects on climate of anthropogenic sulfate aerosols between the 20th and the 21st century. Geophys Res Lett 32: doi: 10.1029/2005GL023619

Dukowicz JK, Baumgardner JR (2000) Incremental remapping as a transport/advection algorithm. J Comput Phys 160: 318-335

Feichter J, Kjellström E, Rodhe H, Dentener F, Lelieveld J, Roelofs GJ (1996) Simulation of the tropospheric sulfur cycle in a global climate model. Atmos Environ 30: 1693-1707

Fogli, PG, co-authors (2009) INGV-CMCC Carbon: A Carbon Cycle Earth System Model, CMCC RP0061 (http://www.cmcc.it/publications-meetings/publications/research-papers/rp0061-ingv-cmcc-carbon-icc-a-carbon-cycle-earth-system-model)

Friedlingstein P, Cox P, Betts R, Bopp L, von Bloh W, Brovkin V, Cadule P, Doney S, Eby M, Fung I, Bala G, John J, Jones C, Joos F, Kato T, Kawamiya M, Knorr W, Lindsay K, Matthews HD, Raddatz T, Rayner P, Reick C, Roeckner E, Schnitzler KG, Schnur R, Strassmann K, Weaver AJ, Yoshikawa C, Zeng N (2006) Climate-carbon cycle feedback analysis: Results from the C4MIP model intercomparison. J Clim 19: 3337-3353

Furevik T, Bentsen M, Drange H, Kindem IKT, Kvamsto NG, Sorteberg A (2003) Description and evaluation of the Bergen climate model: ARPEGE coupled with MICOM. Clim Dyn 21: 27-51

Gibelin AL, Déqué M (2003) Anthropogenic climate change over the Mediterranean region simulated by a global variable resolution model. Clim Dyn 20: 327-339

Gordon C, Cooper C, Senior CA, Banks H, Gregory JM, Johns TC, Mitchell JFB, Wood RA (2000) The simulation of SST, sea ice extents and ocean heat transports in a version of the Hadley Centre coupled model without flux adjustments. Clim Dyn 16: 147-168

Hasselmann K, Sausen R, Maier-Reimer E, Voss R (1993) On the cold start problem in transient simulations with coupled atmosphere-ocean models. Clim Dyn 9: 53-62

Hewitt CD, Griggs DJ (2004) Ensembles-based predictions of climate change and their impacts (ENSEMBLES). EOS Trans AGU 85: 566

Hibbard KA, Meehl GA, Cox PM, Friedlingstein P (2007) A strategy for climate change stabilization experiments. EOS Trans AGU 88: 217-221

Hibler WD III (1979) A dynamic thermodynamic sea ice model. J Phys Oceanogr 9: 815-846

Hourdin F, Musat I, Bony S, Braconnot P, Codron F, Dufresne JL, Fairhead L, Filiberti MA, Friedlingstein P, Grandpeix JY, Krinner G, Levan P, Li ZX, Lott F (2006) The LMDZ4 general circulation model: Climate performance and sensitivity to parametrized physics with emphasis on tropical convection. Clim Dyn 27: 787-813

Huebener H, Cubasch U, Langematz U, Spangehl T, Niehorster F, Fast I, Kunze M (2007) Ensemble climate simulations using a fully coupled ocean-troposphere-stratosphere general circulation model. Phil Trans Roy Soc London A 365: 2089-2101

Janic ZI (1977) Pressure gradient force and advection scheme used for forecasting with steep and small scale topography. Contrib Atmos Phys 50: 186-199

Johns TC, Durman CF, Banks HT, Roberts MJ, McLaren AJ, Ridley JK, Senior CA, Williams KD, Jones A, Rickard GJ, Cusack S, Ingram WJ, Crucifix M, Sexton DMH, Joshi MM, Dong BW, Spencer H, Hill RSR, Gregory JM, Keen AB, Pardaens AK, Lowe JA, Bodas-Salcedo A, Stark S, Searl Y (2006) The new Hadley Centre Climate Model (HadGEM1): Evaluation of coupled simulations. J Clim 19: 1327-1353

Jones A, Roberts DL, Woodage MJ, Johnson CE (2001) Indirect sulphate aerosol forcing in a climate model with an interactive sulphur cycle. J Geophys Res (Atmos) 106: doi: 10.1029/2000JD000089

Joos F, Plattner GK, Stocker TF, Marchal O, Schmittner A (1999) Global warming and marine carbon cycle feedbacks on future atmospheric CO2. Science 284: 464-467

Jungclaus JH, Keenlyside N, Botzet M, Haak H, Luo JJ, Latif M, Marotzke J, Mikolajewicz U, Roeckner E (2006) Ocean circulation and tropical variability in the coupled model ECHAM5/MPI-OM. J Clim 19: 3952-3972

Keen AB, Murphy JM (1997) Influence of natural variability and the cold start problem on the simulated transient response to increasing CO2. Clim Dyn 13: 847-864

Kiehl JT, Schneider TL, Portmann RW, Solomon S (1999) Climate forcing due to tropospheric and stratospheric ozone. J Geophys Res (Atmos) 104: 31239-31254

Klein Goldewijk K (2001) Estimating global land use change over the past 300 years: The HYDE Database. Global Biogeochem Cycles 15: 417-433

Krinner G, Viovy N, de Noblet-Ducoudré N, Ogée J, Polcher J, Friedlingstein P, Ciais P, Sitch S, Prentice IC (2005) A dynamic global vegetation model for studies of the coupled atmosphere-biosphere system. Global Biogeochem Cycles 19: doi: 10.1029/2003GB002199

Legutke, S. and Voss, R. 1999. The Hamburg atmosphere–ocean coupled climate circulation model ECHO-G. DKRZ Technical report no. 18, Deutsches Klimarechenzentrum, Hamburg, Germany

Lowe JA, Hewitt CD, van Vuuren DP, Johns TC, Stehfest E, Royer JF, van der Linden PJ (2009) New study for climate modeling, analyses, and scenarios. EOS Trans AGU 90: 181-182

Madec, G., Delecluse, P., Imbard, I. and Levy, C. (1999): OPA 8.1 Ocean General Circulation Model reference manual. Note du Pôle de modélisation No. 11, Inst. Pierre-Simon Laplace (IPSL), France, 91 pp

Maier-Reimer E (1993) Geochemical cycles in an Ocean General Circulation Model: Preindustrial tracer distributions. Global Biogeochem Cycles 7: 645-677

Maier-Reimer E, Kriest I, Segschneider J, Wetzel P (2005) The Hamburg Ocean Carbon Cycle Model HAMOCC5.1 – Technical description release 1.1. Reports on Earth System Science 14, ISSN 1614-1199 [available from Max Planck Institute for Meteorology, Bundesstr. 53, 20146 Hamburg, Germany, http://www.mpimet.mpg.de], 50pp

Manzini E, McFarlane NA (1998) The effect of varying the source spectrum of a gravity wave parameterization in a middle atmosphere general circulation model. J Geophys Res (Atmos) 103: doi: 10.1029/98JD02274

Marsland SJ, Haak H, Jungclaus JH, Latif M, Röske F (2003) The Max-Planck-Institute global ocean/sea ice model with orthogonal curvilinear coordinates. Ocean Modelling 5: 91-127

Marti O, Braconnot P, Dufresne J-L, Bellier J, Benshila R, Bony S, Brockmann P, Cadule P, Caubel A, Codron F, de Noblet N, Denvil S, Fairhead L, Fichefet T, Foujols M-A, Friedlingstein P, Goosse H, Grandpeix J-Y, Guilyardi E, Hourdin F, Idelkadi A, Kageyama M, Krinner G, Lévy C, Madec G, Mignot J, Musat I, Swingedouw D, Talandier C (2009). Key features of the IPSL ocean atmosphere model and its sensitivity to atmospheric resolution. Clim Dyn: doi: 10.1007/s00382-009-0640-6

McDougall TJ, Jackett DR (2005) An assessment of orthobaric density in the global ocean. J Phys Oceanogr 35: 2054-2075

Otterå OH (2008) Simulating the effects of the 1991 Mount Pinatubo volcanic eruption using the ARPEGE atmosphere general circulation model. Adv Atmos Sci 25: 213-226

Otterå OH, Bentsen M, Bethke I, Kvamstø NG (2009a) Simulated pre-industrial climate in Bergen Climate Model: Model description and large-scale circulation features. Geosci Model Dev Disc 2: 507-549

Otterå OH, Bentsen M and Suo L (2009b) Natural forcing as a pacemaker for Atlantic multidecadal variability. (manuscript in preparation)

Pongratz J, Reick C, Raddatz T, Claussen M (2008) A reconstruction of global agricultural areas and land cover for the last millennium. Global Biogeochem Cycles 22: doi: 10.1029/2007GB003153

Pongratz J, Reick CH, Raddatz T, Claussen M (2009) Effects of anthropogenic land cover change on the carbon cycle of the last millennium. Global Biogeochem Cycle: doi: 10.1029/2009GB003488

Pope VD, Gallani ML, Rowntree PR, Stratton RA (2000) The impact of new physical parametrizations in the Hadley Centre climate model: HadAM3. Clim Dyn 16: 123-146

Quaas J, Boucher O (2005) Constraining the first aerosol indirect radiative forcing in the LMDZ GCM using POLDER and MODIS satellite data. Geophys Res Lett 32: doi: 10.1029/2005GL023850

Raddatz TJ, Reick CH, Knorr W, Kattge J, Roeckner E, Schnur R, Schnitzler KG, Wetzel P, Jungclaus J (2007) Will the tropical land biosphere dominate the climate-carbon cycle feedback during the twenty-first century? Clim Dyn 29: 565-574

Ramankutty N, Foley JA (1999) Estimating historical changes in land cover: North American croplands from 1850 to 1992. Global Ecol Biogeogr 8: 381-396

Roeckner, E., K. Arpe, L. Bengtsson, M. Christoph, M. Claussen, L. Dümenil, M. Esch, M. Giorgetta, U. Schlese, and U. Schulzweida, 1996 The atmospheric general circulation model ECHAM4: Model description and simulation of present-day climate. Max Planck Institut für Meteorologie, Report No. 218, Hamburg, Germany

Roeckner E, Brokopf R, Esch M, Giorgetta M, Hagemann S, Kornblueh L, Manzini E, Schlese U, Schulzweida U (2006) Sensitivity of simulated climate to horizontal and vertical resolution in the ECHAM5 atmosphere model. J Clim 19: 3771-3791

Royer JF, Cariolle D, Chauvin F, Déqué M, Douville H, Hu RM, Planton S, Rascol A, Ricard JL, Salas y Mélia D, Sevault F, Simon P, Somot S, Tyteca S, Terray L, Valcke S (2002) Simulation des changements climatiques au cours du 21-ème siècle incluant l'ozone stratosphérique (Simulation of climate changes during the 21-st century including stratospheric ozone). C R Geoscience 334: 147-154

Salas Mélia D (2002) A global coupled sea ice-ocean model. Ocean Modelling 4: 137-172

Salas-Mélia D., Chauvin F., Déqué M., Douville H., Guérémy J.F., Marquet P., Planton S., Royer J.F., Tyteca S., 2005. Description and validation of CNRM-CM3 global coupled climate model, Note de Centre du GMGEC N°103, décembre 2005. (available from: http://www.cnrm.meteo.fr/scenario2004/paper_cm3.pdf)

Sato M, Hansen JE, McCormick MP, Pollack JB (1993) Stratospheric aerosol optical-depths, 1850-1990. J Geophys Res - Atmos 98: 22987-22994

Sitch S, Smith B, Prentice IC, Arneth A, Bondeau A, Cramer W, Kaplan JO, Levis S, Lucht W, Sykes MT, Thonicke K, Venevsky S (2003) Evaluation of ecosystem dynamics, plant geography and terrestrial carbon cycling in the LPJ dynamic global vegetation model. Glob Change Biol 9: 161-185

Sitch S, Huntingford C, Gedney N, Levy PE, Lomas M, Piao SL, Betts R, Ciais P, Cox P, Friedlingstein P, Jones CD, Prentice IC, Woodward FI (2008) Evaluation of the terrestrial carbon cycle, future plant geography and climate-carbon cycle feedbacks using five Dynamic Global Vegetation Models (DGVMs). Glob Change Biol 14: 2015-2039

Solanki SK, Krivova NA (2003) Can solar variability explain global warming since 1970? J Geophys Res (Space Phys) 108: 1200

Solomon S, Qin D, Manning M, Chen Z, Marquis M, Averyt KB, Tignor M, Miller HL, eds (2007) Climate Change 2007: The Physical Basis. Contribution of Working Group I to the Fourth Assessment Report of the Intergovernmental Panel on Climate Change. Cambridge University Press, Cambridge, United Kingdom and New York, NY, USA, 996 pp

Sovde OA, Gauss M, Smyshlyaev SP, Isaksen ISA (2008) Evaluation of the chemical transport model Oslo CTM2 with focus on Arctic winter ozone depletion. J Geophys Res - Atmos 113: D09304

Stenchikov G., K. Hamilton, R.J. Stouffer, A. Robock, V. Ramaswamy, B. Santere, H.-F. Graf, (2006) Arctic oscillation response to volcanic eruptions in the IPCC AR4 climate models. J. Geophys. Res., 111, D07107, doi :10.1029/2005JD006286.

Terray L, Thual O (1995) OASIS : le couplage océan-atmosphère. La Météorologie N°10: 50-61

Terray L, Thual O, Belamari S, Déqué M, Dandin P, Delecluse P, Lévy C (1995) Climatology and interannual variability simulated by the ARPEGE-OPA coupled model. Clim Dyn 11: 487-505

Timmermann R, Goosse H, Madec G, Fichefet T, Ethe C, Dulière V (2005) On the representation of high latitude processes in the ORCA-LIM global coupled sea ice-ocean model. Ocean Modelling 8: 175-201

Tjiputra J, Assmann K, Bentsen M, Bethke I, Otterå OH, Sturm C, Heinze C (2009) Assessment of regional climate-carbon cycle feedbacks using the Bergen earth system model (BCM-C). Geosci Model Dev Discuss 2: 845-887.

Valcke, S. (2006): OASIS3 User Guide (prism_2-5), PRISM Report No 2, 6th Ed., CERFACS, Toulouse, France, 64 pp

Vichi M, Masina S, Navarra A (2007) A generalized model of pelagic biogeochemistry for the global ocean ecosystem. Part II: Numerical simulations. J Mar Systems 64: 110-134

Vichi, M. et al., 2009: The role of the ocean carbon cycle in the regulation of anthropogenic carbon emissione (manuscript in preparation)

Wolff, JO., Maier-Reimer, E., Legutke, S. 1997 The Hamburg ocean primitive equation model. DKRZ Technical report no. 13, Deutsches Klimarechenzentrum, Hamburg, Germany